

DTIC FILE COPY

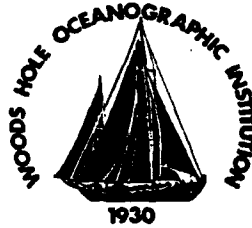
2

WHOI-88-33

AD-A199 529

Woods Hole Oceanographic Institution

DTIC
ELECTE
OCT 1 1 1988
S D
WD



Underwater Imaging System Performance Characterization

by

Jules S. Jaffe

August 1988

Technical Report

Funding was provided by the Office of Naval Research
under contract Number N00014-86-C-0344.

Approved for public release; distribution unlimited.

88 10 7 086

WHOI-88-33

**Underwater Imaging System
Performance Characterization**

by

Jules S. Jaffe

Woods Hole Oceanographic Institution
Woods Hole, Massachusetts 02543

August 1988

Technical Report

Funding was provided by the Office of Naval Research
through contract Number N00014-86-C-0344.

Reproduction in whole or in part is permitted for any purpose of the
United States Government. This report should be cited as:
Woods Hole Oceanog. Inst. Tech. Rept., WHOI-88-33.

Approved for publication; distribution unlimited.

Approved for Distribution:



Albert J. Williams III, Chairman
Department of Ocean Engineering

Underwater Imaging System Performance Characterization

Jules S. Jaffe

Department of Ocean Engineering
Woods Hole Oceanographic Institution
Woods Hole, MA 02543



Accession For	
NTIS CRA&I	<input checked="" type="checkbox"/>
DTIC TAB	<input type="checkbox"/>
Unannounced	<input type="checkbox"/>
Justification	
By _____	
Distribution _____	
Availability Codes	
Dist	Availability or Statement
A-1	

Contents

1	Introduction	1
2	Computer Simulation of Underwater Images	2
2.1	The Physics of Underwater Image Formation	2
2.2	The UNCLES Computer Modeling System	4
2.3	The Direct and Forward Scattered Component	5
2.4	The Backscatter Component	7
2.5	Relating UNCLES Output to System Performance	9
2.6	A Sample UNCLES Run	11
3	Vehicle Characterization Study	13
4	Advanced Imaging Concepts	17
4.1	Range-Gated Imaging	17
4.2	Scanned White Light Stripe Performance	20
5	Ambient Lighting Study	21
6	Parameter Sensitivity Study	23

1 Introduction

The correct design of underwater camera systems for viewing underwater objects is vitally important if the performance of these underwater imaging systems is to be maximized. Towards this goal, the Woods Hole Oceanographic Institution has developed a system of computer programs which allows the underwater lighting system designer to explore the imaging system performance that results from the manipulation of beam patterns, geometry of cameras and light sources, and changes in the environment.

The computer simulation of underwater image system performance has been found to be a valuable tool for several reasons. Most importantly, the performance of underwater lighting systems cannot be easily predicted from terrestrial experience because of the intense scattering of the oceanic medium. Secondly, the cost of implementing and running computer programs to simulate underwater camera light viewing is at greatly reduced expense to experimentation in the real world. Finally, the inherent flexibility in using a computer for modeling allows the user to build up a base of experience which can then be used for heuristic system design.

In this report, we will consider the results of a systematic study that was performed in order to quantify and refine the performance of an underwater imaging system. The camera and lighting system of the mine neutralization system (MNS) was subject to an intensive computer study of over 500 simulations in order to characterize the existing system performance and to determine the scope of both simple and more complex changes that could be made in order to optimize the performance of the imaging system.

Figure 1 is a page from a document which details the MNS performance. As documented, it is evident that the mission requirement of the vehicle is to neutralize either bottom or moored mines, once they have been located by some other device. In the bottom neutralization mode, the MNS deploys a small bomblet within a given radius of the mine which is then detonated

after the vehicle has swum a safe distance away. The primary requirement here is that the optical imaging system of the MNS be able to locate the mine from a safe distance. Therefore, the greater the stand-off distance, the better the vehicle performance.

In clear water conditions, where underwater visibility may cover quite large distances, the system should be able to satisfy the mission requirements. However, in many coastal regions the underwater visibility of objects can be hampered by the presence of absorptive and scattering matter in the water column. In these situations, any improvement in vehicle performance would be advantageous, as the chances for detonation of the underwater mine would be reduced. In this study we will detail a suite of possible options that are available to the MNS. These options range from some that are extremely simple such as moving the lights, to more complex options which will result in larger payoffs in improved vehicle performance.

2 Computer Simulation of Underwater Images

2.1 The Physics of Underwater Image Formation

In this report, we will be concerned with the propagation of electromagnetic waves in isotropic, homogeneous media. In this situation, the two basic ways that light interacts with matter are via attenuation and scattering. The attenuation coefficient for pure water is predicted via Maxwell's equations to be related to the complex part of the complex index of refraction. Absorption can also occur due to the concentration of pigmented species in the water. Scattering can be defined as any divergence from a straight line path. In the underwater realm light can either be diffracted by particles that are on the order of the wavelength of the light, or refracted by particulate matter that has a different index of refraction than the surrounding sea or lake water.

Empirically, these phenomena can be grouped together via measurement. The total absorption coefficient c is the decay constant that is associated with the removal of light intensity per unit distance:

$$I(r) = I(o)e^{-cr} \quad (1)$$

Here, r is distance and I is the irradiance at positions $I(o)$ and $I(r)$.

The constant c can be further decomposed as a sum of two quantities, the absorption and scattering coefficients so that:

$$c = a + b \text{ and } I = I(o)e^{-ar} e^{-br} \quad (2)$$

The above treatment is precisely the case for an infinitely small, thin beam where no radiation is scattered back into the beam. In this case, all scattering and absorption events lead to the loss of light flux. Transmissometers measure an approximate value of c by maintaining a very small diameter beam.

The total scattering coefficient, b , is the superposition of all scattering events at all angles. It can be viewed as the integral of the volume scattering function $\beta(\theta)$ over all solid angle:

$$b = \int_0^\pi \beta(\theta)dw = 2\pi \int_0^\pi \beta(\theta)\sin\theta d\theta \quad (3)$$

The four quantities, a , b , c , and $\beta(\theta)$, represent the inherent properties of the medium. They are distinct from the apparent properties as they do not depend on the radiance field about a measurement point [Priesendorfer, 1976]. In principle, these quantities are all that one needs in order to predict the propagation of light underwater.

2.2 The UNCLES Computer Modeling System

The approach that we have been pursuing is related to a model formulated by McGlamery and coworkers at the Scripps Institute of Oceanography Visibility Laboratory [McGlamery,1979]. The model can be described as a hybrid approach in that linearization is incorporated in certain situations in order to simplify the computation. When this approximation cannot be made the quantities of interest are calculated explicitly.

As illustrated in Figure 2, an underwater imaging experiment consists of tracing the progression of light from a light source to a camera. Several pathways exist by which the light can travel to the image plane of the camera. These pathways may or may not include light that has been reflected by an object. Therefore, the light that has entered the camera may or may not have been reflected by the object. The light that enters the camera without reflection from the object gives rise to an imaging component that is called backscatter. Considering the light reflected by the object, we can distinguish two components that are incident upon the camera plane: 1)light that has not been scattered in the intervening water, called the direct component, and 2)light that has been small angle scattered, called the forward scattered component. We choose to represent an image as being the linear superposition of three components: 1)backscatter, 2)forward scattering, and, 3)a direct component. These pathways are illustrated in Figure 2. Mathematically,

$$E_T(\text{total}) = E_d(\text{direct}) + E_{f_s}(\text{forwardscatter}) + E_{b_s}(\text{backscatter}) \quad (4)$$

2.3 The Direct and Forward Scattered Component

In order to calculate the light reflected from the map, the irradiance pattern incident upon the reflectance map must first be calculated. The origin of this irradiance is the light source, considered here to be a point source characterized by a beam pattern $BP(\theta, \varphi)$, a function of polar angles θ , and φ . In order to calculate the radiance incident upon the map this beam pattern is geometrically projected. As a final approximation, the scalar irradiance incident upon the reflectance map can then be calculated as:

$$E'_I(x', y', \theta, \varphi) = BP(\theta, \varphi) \cos \gamma \frac{e^{-cR_s}}{R_s^2} \quad (5)$$

Here, x', y' refer to the fixed coordinate system with respect to the planar reflectance map located at $z' = 0$. $R_s(x, y, z, x', y', 0)$ is the distance from the source to a point on the reflectance map and γ is the angle between a perpendicular to the reflectance map at a given x', y' location and a line between the x', y' location and the source. The constant c is the total attenuation coefficient. The geometry is illustrated in Figure 2. Note that the primed coordinate system is associated with the reflectance map and the unprimed coordinate system is associated with the camera plane. A more accurate representation of the incident irradiance, E_I takes into account the spreading of illumination due to the small angle forward scattered component. An approximate value can be found via a convolution with a point spread function as is typical in image processing [Rosenfeld and Kak:1982]. In this case,

$$E_I(x', y', 0) = E'_I(x', y', 0) * g(R_s, G, c, B) + E'_I(x', y', 0) \quad (6)$$

where

$$g(R_s, G, c, B) = \{ \exp(-GR_s) - \exp(-cR_s) \} F^{-1} \exp(-BR_s f) \quad (7)$$

and G is an empirical constant ($|G| \leq c$). The operator F^{-1} indicates that an inverse Fourier transform is taken of a function B , an empirical damping factor, and f , a radial frequency in cycles/radian. Wells [1969] has shown that in the small angle scattering approximation, the linear relationship of equation (3) is valid. This is equivalent to the formulation proposed by McGlamery [1979]. It is also justifiable on a more theoretical basis as considered in the treatment of Gordon [1973]. In Gordon's work, the relationship was found to agree with Monte Carlo calculations for distances of up to 6 attenuation lengths.

In order to compute the reflected radiance, the values of the incident irradiance pattern are multiplied by the reflectance values of the reflectance map. In the UNCLES system an object is represented by a planar reflectance map $M(x', y')$ located in 3-dimensional space at a given orientation. Note that $M(x', y') \leq 1$. Typical values for objects of oceanographic interest are $.02 \leq M(x', y') \leq .1$ [Dixon et.al.;1983]. In addition, a geometric factor of $\cos\theta$ is taken into consideration in accordance with Lambert's law. The angle θ is the angle between a normal to the reflectance map at position x', y' , and the camera aperture as illustrated in Figure 2.

In order to predict the scalar irradiance incident upon the image plane of the camera it is necessary to consider the geometric optics of the camera, the attenuation of the medium between the reflectance map and the camera, and the spherical spreading of the reflected wave. Taking these factors into consideration, the scalar irradiance incident upon the image plane of the camera can be represented as:

$$E_d(x, y) = E_I(x', y') \exp(-cR_c) \frac{M(x', y')}{4f_n} \cos^4 \theta T_l \left[\frac{R_c - F_l}{R_c} \right]^2 \quad (8)$$

where R_c is the distance from an x', y' position on the reflectance map to the camera. f_n is the f number of the camera of focal length F_l , and T_l is the transmittance of the lens.

The forward scattered component can then be calculated from the direct component via the convolution relationship:

$$E_{fs}(x, y) = E_d(x, y, o) * g(R_c, G, c, B.) \quad (9)$$

where g is represented by equation [7].

2.4 The Backscatter Component

The calculation of the backscatter component is the most computationally intense part of the computer program. This is because the linear approximation is no longer valid as the backscattered light enters the camera from a large distribution of angles. Alternatively stated, the small angle approximation used in making the linear approximation in computing the forward scattered component is no longer valid.

The approach taken in this work follows that of McGlamery in that 3-dimensional space is sliced into planes of thickness $\Delta z'$ that are parallel to the image plane of the camera. The irradiance incident upon each of these planes is then calculated, as above, by computing the direct component and then adding an additional amount of irradiance due to the light that is small angle scattered.

The next step in computing the backscatter component is to determine the resulting image due to each of these illuminated slabs. The irradiance incident upon the aperture of

the camera is a superposition of these illuminated volume elements weighted by the value of the volume scattering function. Representing the scalar irradiance in 3-dimensional space propagating away from the light source as $E_s(x', y', z')$, following the above arguments:

$$E_s(x', y', z') = E_{s,d}(x', y', z') + E_{s,f_s}(x', y', z') \quad (10)$$

$$E_{s,d}(x', y', z') = BP(\theta, \varphi) \frac{\exp(-cR_s)}{R_s^2} \quad (11)$$

$$E_{s,f_s}(x', y', z') = E_{s,d}(x', y', z') * g(R_s, G, c, B) \quad (12)$$

Now, taking a weighted superposition of the intensities from a given slice, we can compute the radiant intensity that is scattered toward the camera element x, y due to volume $\Delta V'$:

$$H_{bs}(\varphi, x, y) = \beta(\varphi) E_s(x', y', z') \Delta V' \quad (13)$$

where $\beta(\varphi)$ represents the volume scattering function and $\Delta V'$ is an incremental volume in 3-dimensional space. The angle φ is between a line from the volume under consideration to the light source and a line from the volume to the camera. Next, the image of this volume of water must be calculated. In this case, following arguments similar to those above, the direct component of this backscattered scalar irradiance, $E_{bs,d}(x, y)$, can be represented [McGlamery, 1979] as:

$$E_{bs,d}(x, y) = \sum_{i=1}^N \exp(-cZ_{ci}) \beta(\theta) E_s(x', y', z') \frac{\pi \Delta Z'}{4f_n^2} \cos^3 \theta T_l \left[\frac{Z_{ci} - f_l}{Z_{ci}} \right]^2 \quad (14)$$

Here, $\Delta Z'$ is the thickness of the backscattering volume $\Delta V'$. Z_{ci} is the distance from a point in the camera to the center of the backscatter slab. The value N extends from $i = 1$ for the first backscatter plane to N for the plane adjacent to the target. As noted previously,

the total scalar irradiance due to the backscattered image , $E_{bs}(x, y)$, can then be calculated by adding an additional forward scattered component:

$$E_{bs}(x, y) = E_{bs,d}(x, y) + E_{bs,d}(x, y) * g(R_c, G, c, B) \quad (15)$$

2.5 Relating UNCLES Output to System Performance

In evaluating the performance of an underwater imaging system there are two important criteria that must be considered. One of these is whether the amount of power falling upon the sensing device is large enough to be able to allow adequate signal to noise levels in the image. In addition, the contrast in the image must be assessed in order to evaluate whether the resultant image contains visible features.

In the case of the power levels, adequate power incident upon the sensor can be calculated via a *straightforward conversion of UNCLES output values*. Several factors must be taken into account in order to compute the amount of photon flux that is incident upon the aperture of the camera. In this situation, we have employed the approach taken by the Navy underwater imaging handbook [Funk et.al. 1973].

In order to determine the power levels incident upon the image plane of the camera, a conversion formula has been used to convert from the output of the UNCLES program M_c which is the value for a one watt lighting source.

$$E_c = M_c * P_s * N_s * N_w * N_r \quad (16)$$

Here, E_c is the output value in lux, P_s is the amount of power output by the illuminating device integrated over 1 second (assuming a one second exposure), N_s is the photometric

output of the illumination source, N_w is the water radiant efficiency transfer, and N_r is the efficiency of the reflector (only useful for strobe illumination).

Standard values of N_w can be found in the Navy handbook. This value is a function of the spectral characteristics of the lighting source, the distance between the source and the camera, and the attenuation constant of the water. The value of N_w reflects how the water passes the different spectral bands of the lighting source. For a blue-green laser, the value would be larger than that of a longer wavelength source which contains light that is attenuated more rapidly. Although the UNCLES system is essentially monochromatic, by using the appropriate values here, the spectral dependency of the attenuation can be considered in computing the incident power. Table 1 contains the values of the power conversion units that should be used for this study. Here we have tabulated the conversion factor from UNCLES output to radiometric intensity for incandescent, and thalium iodide lighting sources. The left hand column indicates the number of attenuation lengths and the headings indicate the water type. Note that the thalium iodide source has the greatest conversion efficiency factor. This is because the spectral characteristics of the light source match the pass-band characteristics of the water closely.

A more difficult area that must be taken into consideration in order to evaluate image quality is the contrast transmittance. Defining this quantity as the fraction of direct light that is incident upon the camera plane, it can be represented as:

$$C_t = \frac{E_d}{E_d + E_{fs} + E_{bs}} \quad (17)$$

A minimal level of contrast is necessary in order for the human observer to discriminate target from background. Our own experiments with the UNCLES system have led us to

conclude that a value of .02 contrast transmittance is adequate for viewer discrimination. Furthermore, an acceptable image will be defined when this value occurs over greater than 25 percent of the viewing area. In summary, the criteria for adequate image visibility is: (1) a power level which allows the video camera to image the scene in its linear range, and (2) a contrast value which is greater than .02 over at least 25 percent of the field of view.

2.6 A Sample UNCLES Run

In this section a sample UNCLES input data set and the resultant output of the program will be illustrated. The sample input data file is contained in Table 2. Here we see that the input to the system of computer programs consists of several distinct sections. The first set of input data are the constants that describe the environmental parameters. The total attenuation coefficient ($c = a + b$), the scattering to attenuation ratio, $\frac{b}{a+b}$, the empirical constants relating to the scattering power and the loss of resolution as a function of distance are the first four parameters. The volume scattering function (VSF) is next input. An illustration of a slice through this radially symmetric function is contained in Table 2.

The next set of input variables relate to the characteristics of the camera. The x and y focal planes, f_n (f number of the lens), and the camera lens focal length are all needed for the computations. The beam pattern functions are input next. Here, a file containing the angular dependence of the power of the beam, the total integrated power in the beam (always set to 1 in the simulations considered here), the beam pattern width (used for the striped illumination) and the source pulse length in nanoseconds for range gating (a value of 0 implies a continuous source) are the next set of variables that need to be included.

In order to specify the reflectance map pattern a 2-dimensional file is required. The file-name is an input variable to the UNCLES system. Additional values needed in order to

characterize the location and the length of the reflectance map are its center x and y coordinates, its length in the x and y direction, and the number of x and y picture elements (pixels) that the map contains. Additional information is a value for the reflectance of the background, assumed to be the area surrounding the reflectance map.

Three sets of locations, and the Eulerian angles associated with the orientations of the camera, and the two sources are needed in order to compute the resultant images. In addition, the number of rows and columns in the final image are input. Several options used in the computations also exist. Auto-aim negates the need to calculate all of the angles and points the lights and the camera at the center of the reflectance map. The options for the convolutions are provided to allow computation as Fast Fourier Transforms or direct convolutions in image space. The latter provides zero padding and eliminates, any wrap-around effects at the expense of computation time.

Finally, a recent addition to the program allows the input of a vehicle which is specified as a set of polygons bounded by vertices. The vehicle file contains the number of vertices and their coordinates in three dimensional space. This option provides the ability to specify baffles on the vehicle which can be helpful in order to reduce the amount of backscatter.

The program is then invoked in an interactive, menu driven mode, and the user is asked to verify the correctness of the input by observing the predicted values of the illumination and the field of view of the camera in the target plane. If these values are acceptable the program is then executed and an output file containing matrices, of the illumination pattern, the direct, glow, backscatter and total image components, and the contrast transmittance are all recorded. We have found that by viewing contour plots of these matrices valuable information about the distribution of the values can be interpreted. As an example, considering the simulation described above, a contour plot of the total component is illustrated in Figure 3

and the contrast transmittance in Figure 4.

In addition, a useful method of display is to generate graphs of lines through the two-dimensional data. For example, a row or column can be specified and the values of the total, backscatter, forward scatter, and the direct component can be graphed along that coordinate. This is illustrated in Figure 5 for a central row of the image. The advantage of this form of presentation is that the dynamic range of the image components can be easily inferred. Finally, the program generates a new parameter file which can either be reused for program input, or saved as documentation. An additional note on the parameter file is that the scaling constants are recorded that were used in order to constrain the output matrix values between 0 and 255.

3 Vehicle Characterization Study

In order to suggest changes to increase the performance of the MNV system, the first task to be accomplished was to enter all of the relevant system parameters into the computer program. This included the locations of the existing lights, the cameras, and the beam patterns of the lights. This information was obtained from the engineering drawings provided to WHOI by the Naval Coastal System Center (NCSC). Figure 6 shows the configuration of the MNV system as presented in the MNV handbook. Here, we can see that two sets of lamps are provided forward and aft. In this study, we will only be concerned with the aft system. The forward set of lamps are of no interest for long range viewing in that they create a great deal of backscatter which obscures the appearance of underwater objects.

In addition to the physical location of the cameras and lights, the environmental circumstances in which the vehicle might find itself were considered. Since the vehicle is intended to be used in coastal regions, the major emphasis was placed on examining the system per-

formance in poor visibility conditions. Towards this end, a systematic study of contrast transmittance and power requirements over the possible operating situations of interest were compiled using the UNCLES program.

Figure 7 represents a summary of the entire first part of the study. In this figure the achievable altitude of the vehicle has been graphed versus the total attenuation coefficient of the water. The points on this graph were determined in the following manner: first, a set of computer runs were performed at various altitudes for a given water attenuation value. In this case, we chose to investigate total inverse attenuation coefficients of 3.3, 6.6, and 20 m. Then, the altitude at which .02 contrast transmittance occurred over 25% of the image was estimated by interpolating the percentage values from multiple computer runs at different altitudes. The results of these computer runs are contained in graphs 7a, 7b, and 7c. The key for all of the simulation in this study are listed in Table 4.

In this section we are interested in the two lowest graphs in the figure. The viewing altitude is depicted on the graph for the original configuration of the vehicle in two situations, one where the reflectance of the background was .02 and the other where the background reflectance value was .1. Information provided to us from NCSC indicated that these values would be realistic for various underwater imaging scenarios. As can be seen from the illustrations, the practical performance limitations of the current system for the low contrast background are to limit the observability of the bottom to 5 meters distance in 3.3 meter water, 8.5 meter distance in 6.6 meter water, and 19 meter distance in 20 meter water. With a more reflective background of .1, the vehicle is predicted to be able to obtain reasonable images at 7 meter altitude in 3.3 meter water, 10 meter altitude in 6.6 meter water, and at 22 meter altitude in 20 meter water. Thus, the practical limitations of the vehicle limit it to 1.5-2 attenuation lengths in cloudy conditions, and barely more than one attenuation length

in clear water.

Now that the baseline configuration of the vehicle had been determined, a number of simple changes were considered whose aim were to improve the performance of the imaging system. The first change that was considered was to reposition the lights of the vehicle further aft. A convenient place to locate them was found on the vehicle which allowed them to be placed approximately 10 feet back from the camera in the nose of the vehicle. The new imaging performance of the vehicle is contained in Figure 7.

As depicted, a dramatic increase in the imaging performance was evident. In this case, the contrast limited performance at 3.3 meters attenuation was now increased to over 7 meters for the low resolution case and 8.5 meters for the case of the higher background reflectance. As can be seen from the graph, in the 6.6 meter case the new vehicle altitude for the low contrast case is 12.5 meters, and in the higher contrast case, 13.5 meters. In the clear water case, the vehicle altitude could be increased to almost 20 meters in the low contrast case, and to 29 meters in the high contrast case. Note that the imaging performance has been increased in all cases, however, substantially more in the poorer imaging conditions.

The next system modification that was explored was to narrow the beam patterns for the vehicle lamps. The objective here was twofold: 1) concentrate the available lighting power, and 2) decrease the amount of backscatter that is incident on the camera by decreasing the common volume of intersection of the camera and the lights. As can be seen from the Figure 7 system characterization, in all cases this resulted in an increase in the system performance. The greatest increase in the imaging performance occurred in the cloudiest water condition. In the 3.3 meter water the system performance increased to nearly 9 meters, a distance of almost 3 attenuation lengths for the high contrast case. In 6.6 meter water the imaging performance increased to 13 meters. In the 20 meter clear water case, the final imaging distance for the

system was 37 meters.

Additional experiments were performed to determine a set of optimal pointing angles for the computer simulations. In this case, the clearest water conditions were given priority in that this would result in the longest range imaging. As can be seen from the graph, this resulted in maximizing the viewing distance for the 20 meter case, however, in the cloudier conditions the change in pointing angles did not result in the highest image quality. If the imaging system performance were in fact optimized for the poorer water quality, some sacrifice in higher image quality would result. Since the cloudier water conditions limit the performance of the vehicle more severely, this is the direction that would be taken in a future study.

The final study performed in this first phase of the research was to examine the performance and limitations of the lamps and video camera. Table 2 contains a graph of the required power levels for the different imaging configurations in the different water conditions. With respect to this, we note that the incandescent lamps presently on the vehicle will not provide adequate power levels for some of the extended range configurations that we have recommended. Although adequate for the initial imaging range of the vehicle, according to our calculations the new extended configuration will be power limited. Two ways of combating this power limitation would be to increase the efficiency of the lamps, and to also increase the sensitivity of the camera. We recommend that both changes be implemented.

In the case of the lamps, thalium iodide lighting sources provide two advantages for underwater illumination: One, they are more efficient in that they convert more electrical watts to radiant watts than either incandescent or fluorescent. The second advantage is that their output spectra is much better matched to the passband characteristics of the water. These facts are highlighted in Table 1, a listing of conversion factors from UNCLES units which are normalized to one watt output to lux. Here it is seen that as a function of water

type and distance, the thalium iodide lamps can provide a factor of 5 to 7 increase in light power efficiency. In all of the discussions that follow it will be assumed that thalium iodide lamps of the same wattage as the incandescent lamps are to be used.

The sensitivity of the existing camera has also been examined. In Figure 8, a graph of signal output versus camera sensitivity in lux, it is noted that for the newvicon camera which is currently on the vehicle, the expected value of lux for the extended configurations is almost 2 orders of magnitude away from the given sensitivity of the current camera(newvicon). It is therefore recommended that the camera be replaced with a silicon vidicon camera (ultracon).

In summary we have shown that the imaging performance of the vehicle can be approximately doubled in cloudy water conditions by observing the following suite of suggestions:

- 1) move the bottom lights aft to achieve maximal separation between camera and lights.
- 2) change the lights to thalium iodide with concurrent changes in beam patterns(narrowing).
- 3) change the current camera to a more sensitive type(ultracon is recommended for compatibility).

4 Advanced Imaging Concepts

4.1 Range-Gated Imaging

In this section two advanced imaging concepts will be presented. As possible options for the MNV they have the potential to allow longer range imaging than do conventional approaches such as the ones described above. Limitations to conventional underwater lighting systems are due to the severe backscatter component that is present. The methods explored in this section have been proposed to allow increased imaging performance by circumventing the large backscatter contribution.

Range-gating a light source and a receiver is a technique that has been advocated in order to decrease the contribution due to backscatter. The basic idea is that by propagating a short pulse of light, a slab of water of finite thickness will be illuminated. If the receiving device is opened for a time length that is equal to the length of the light pulse, then, by varying the onset time of the device, information about only a thickness of water at a given range will be collected. This technique can be used with any pulsed light source. The idea is illustrated in Figure 9.

We have used an extended version of the UNCLES program to examine the advantages and disadvantages associated with range-gated illumination. The program was extended in order to only allow backscatter to enter the camera from slabs of water that were coincidentally illuminated when light was being reflected from the target. Two sets of simulations were then executed, one corresponding to a pulse length of time equal to 17 ns and another equal to a pulse length equal to 35 ns. In the simulations, it was assumed that the receiving device could be opened for an exactly equivalent amount of time. The advantage of the longer pulse length is that more power can be collected per pulse by the receiving device. The disadvantage of the longer pulse is that the amount of backscatter that is received by the sensor is increased.

An example of the result of using the UNCLES program to simulate the acquisition of a range-gated image is shown in Figure 10. In this case, we have assumed coincident positioning of the camera and the light source. The inverse attenuation coefficient was assumed to be 6.6 meters, and the altitude of the device was assumed to be 28 meters. The image is for a pulse length of 17 nanoseconds. This figure illustrates the large degree of image contrast that can result from the use of a range-gated system. In fact, in all of the cases considered in the simulations, the contrast values were always found to be adequate.

A set of simulations were run for the laser range-gated case as a function of distance and

environmental parameters. The attenuation coefficients that were used were identical to those above. Power computations were then performed in order to determine the radiant intensity values that would be incident on the image plane of the camera. For the blue-green laser a power output level of 35mj was assumed with a pulse repetition rate of 25 pulses/sec. In this case, a conversion factor of 500 watts/lumen was used. Figure 11 contains a graph of the results of the study. As can be seen, the power levels for the longer range images are too small to be sensed by the receiving sensor. Typical values for both SIT cameras and CCD devices are 5×10^{-5} lux [RCA Handbook;1974]. This has led us to conclude that the current possibilities for laser range-gated imaging at large distances are extremely limited.

Figure 11 also contains the resultant power levels that would be seen for a gated strobe lamp with an integration time of 35ns. Here, we have assumed that the spectra of the light source would be similar to that of a Thallium Iodide lamp. It has been assumed that strobe power levels are a value of 250 watts, and that they are capable of delivering a power of 85 lumens/watt of electrical power. In this case, because the water does not pass all bands of the broad spectrum of the light equally, N_w must be determined. This is an empirical factor which is a range dependent, environment dependent efficiency factor. Standard values of these coefficients are itemized in the Navy Handbook .

Finally, in the case of the strobe lamp, the duty cycle for a gated, repetitive, strobe needs to be incorporated in the integrated illumination intensity calculation. The factor for a strobe light repeating illumination with a pulse length of 35 nanoseconds every 4 microseconds would be .009. These values are commensurate with using a gated CID camera[Xybion Co.;1987]. The main disadvantage of incoherent gated illumination, in this respect, is that gating results in extremely inefficient use of illumination. As can be seen, in this case, the power levels at the receiver are less than those due to the laser light above. On the basis of the results of the

computer simulation we note that the laser-gated and range-gated incoherent illumination systems do not hold the possibility for long range viewing. In consideration of these results, other imaging techniques have been formulated in order to see whether improved performance could result.

4.2 Scanned White Light Stripe Performance

In this section a new technique is considered which consists of scanning a stripe of incoherent light across the field of view. The situation is illustrated in Figure 12. Here, as an example, the light source and the camera have been placed on a vehicle of length 5 meters. As is widely recognized, increasing the distance between source and receiver can lead to better images by reducing the common backscatter volume in the final picture. The proposed configuration presented is an extension of that technique. The basic idea consists of forming a narrow strip of illumination athwartships and scanning this stripe along the vehicle axis.

The image of the striped illumination pattern is then recorded on a camera for a fixed period of time. In this example we have used $1/30^{th}$ of a second as it corresponds to a video frame rate. The image can also be acquired by an image processor in the $1/30^{th}$ of a second. The next step consists of using the image processor to detect the boundary of the illuminated area. Knowing the width of the beam and the approximate height of the vehicle, an area of interest can be delineated which corresponds to the area illuminated by the stripe. This region of interest is then numerically dissected out from the received image and added to the contents of another frame buffer. Commercially available devices permit the feedback of images into an accumulation image buffer at this rate.

This process is then continued for the number of individually scanned lines in the picture.

equal to the total image area divided by the width of an individual scan line. In this example, 20 individual scan lines have been delineated which are then summed. The final image consists of a superposition of all of these individual striped images. Finally, contrast enhancement procedures can be used to increase the visibility of such a device, providing the receiving sensor has the available dynamic range. Figure 12 illustrates a flow chart for the system.

The result of using an extended version of the UNCLES program to calculate the performance of such an imaging system is shown in Figure 13. The image simulation was performed at an altitude of 12 meters in $3.3m^{-1}$ water. In this case, to illustrate the performance of such a device, 20 slices were used. Additionally, a gradient threshold was used to trigger the delineation of the region of interest. As can be seen, the contrast in the image is quite adequate for observer recognition of important features. In addition, the mean power levels that are obtainable across the object field are adequate for camera detection. As illustrated we predict that using light striped illumination image visibility to at least 4 attenuation lengths is possible in some situations. We feel that this is a conservative estimate. The ultimate limitations of such a device should be comparable to the performances obtained with synchronous scanned systems, that is, 5-7 attenuation lengths. It is concluded that light striped illumination has superior potential over range-gated techniques in certain long range imaging situations.

5 Ambient Lighting Study

At the request of NCSC a study of ambient lighting situations that might lead to useful imaging conditions was undertaken. System performance specifications for underwater image power and visibility as a function of water type were requested. A modest amount of effort was put into a series of simulations in the hope that the UNCLES model could be used

to predict image performance in various underwater imaging scenarios where ambient light would provide illumination for imaging. The results obtained were suggestive, however not completely satisfactory in that the program was being used in an imaging regime for which it was not intended. The outcome of the simulations are presented here for completeness.

The geometry used to simulate ambient lighting conditions was to suspend the source at an altitude of 200 meters directly above the camera and the target. In this way, approximately parallel illumination could be simulated. Although the actual power in the computed image would not be realistic, it was decided that the relative amount of backscatter could be inferred and therefore that the contrast transmittance levels for the images would be of use. The results of the study, presented in Figure 14, depict a range of contrast transmittance values contained in the image as a function of water type and altitude.

The results indicate that at an altitude of one attenuation length the images will all be of high contrast, the contrast transmittance values being between .3 and .5. When the vehicle is at an altitude of 2 attenuation lengths, the 3.3 and 6.6 meter attenuation constant waters permit adequate image contrast to allow imaging. In the case of 40 meter altitude and 20 meter attenuation coefficient the image contrast will be extremely low. The model also predicts that the images will be of marginal contrast for the 3.3 and 6.6 meter imaging conditions at 3 attenuation lengths of altitude.

These values correspond to the case when the sun is directly overhead and the camera is looking straight down. As a matter of practical experience, experienced divers have noted that in relatively clear waters imaging distances can approach 70 meters. For 20 meter water conditions this corresponds to two and a half attenuation lengths. This performance is greater than that predicted by the UNCLES model. The most likely cause of the discrepancy is that the computer model is only equipped to deal with singly scattered photons. At modest

water depths the ambient light field is more isotropically distributed than that predicted by the computer model. Less backscattered photons therefore enter the camera and, as a result, more object visibility exists. A complete simulation of the limitations of ambient light viewing would need to take these facts into consideration. Under the auspices of the present study this was not possible.

6 Parameter Sensitivity Study

An important issue in the examination of the performance of underwater imaging systems is the characterization of the environment in which the light is propagating. As we have already seen, this requires knowledge of the total attenuation constant, the scattering to attenuation ratios, the volume scattering function, and the empirical constants that relate to the spreading of the beam. A natural question arises in this context : What are the sensitivities in the predicted images to errors in the characterization of these constants?

In order to examine the answer to this question we have performed a limited number of computer simulations to examine the variation in contrast transmittance with respect to variations in the value of the scattering to attenuation ratio and attenuation constant. A full multidimensional simulation would necessarily take into account the systematic variations in almost all image parameters and the resultant changes in the power and contrast transmittance. Since some of the input parameters are complex this full simulation would be extremely consumptive of computer power. Moreover, a quick look at some of the physical relationships indicates which of the parameters should be important.

The result of a set of simulations to characterize the change in contrast transmittance with respect to scattering to attenuation ratio are depicted in Figure 15. Arbitrary image configurations were chosen as starting conditions and small perturbations (10%) in the envi-

ronmental parameters were performed in order to examine the resultant changes in contrast transmittance. As can be seen from the simulations the contrast transmittance values were moderately sensitive to changes in the scattering to total attenuation coefficient value. One measure of this sensitivity of the change is the slope of the line graphed in Table 3. Table 3 outlines the slope versus water conditions for the two sets of simulations performed: contrast transmittance versus attenuation, and contrast transmittance versus scattering to absorption ratios.

As can be seen, the largest relative change in contrast transmittance to attenuation ratio was a value of 2.76. This infers that the degree of accuracy needed in α for a measurement of the contrast transmittance of accuracy .01 (half the threshold value) would be .0036. In the case of the scattering to absorption ratio the contrast was much less sensitive, the largest value being approximately -.7. Here, the accuracy needed in the s/α ratio would be .05. It is therefore recommended that data collection devices be employed which will yield measurements of the total attenuation and absorption to scattering ratios as described above.

letter	meaning in UNCLES filename
U	starting character of UNCLES runs
R	3.3 meter water
S	6.6 meter water
T	20. meter water
(number)	vehicle altitude
A	S/L separation
B	narrow beam
C	new beam direction
M	.1, .02 reflectance map
N	.1 uniform reflectance map
P	.04, .02 reflectance map
Q	.04 <i>uniform reflectance map</i>
I	10% decrease in α
J	10% increase in α
K	30% decrease in $\frac{\beta}{\alpha}$
L	30% increase in $\frac{\beta}{\alpha}$

Table 1:

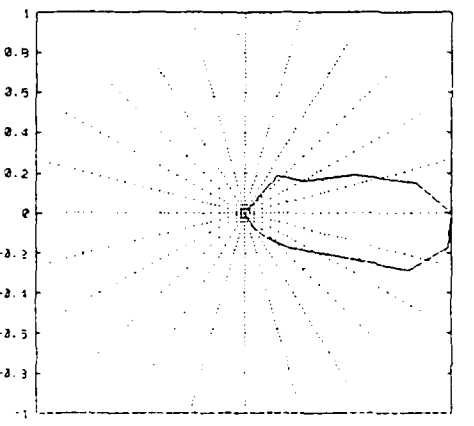
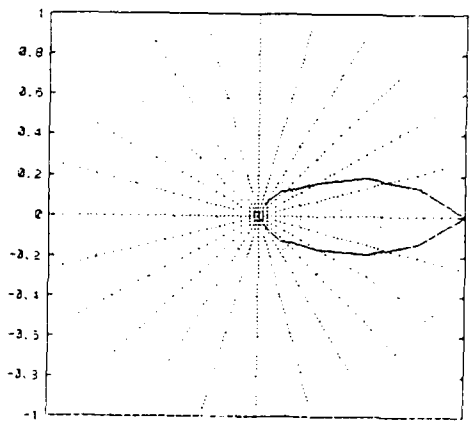
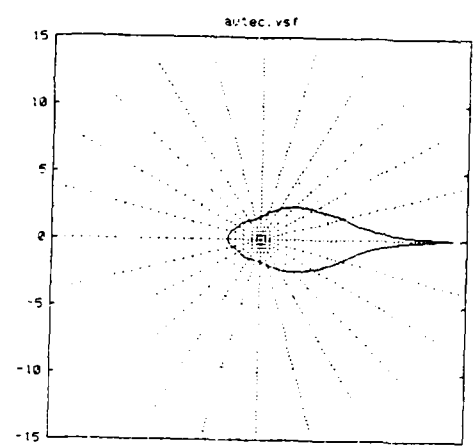
Key To UNCLES Filenames: MNVS Study

***** UNCLES - Underwater Camera-Light Experimentation System *****
 ***** Parameters File *****
 ***** 3/28/1988 17: 4:56 *****

```

Alpha : 0.300000e+00
S/alpha : 0.833000e+00
G : 0.275000e+00
GFSK : 0.100000e+00
V.S.F. filename : autec.vsf
DeltaD : 0.000000e+00
Lambda : 0.000000e+00
Q.E. : 0.000000e+00
Time : 0.000000e+00
FocalplaneX : 0.950000e-02
FocalplaneY : 0.127000e-01
Fnumber : 0.180000e+01
Focal length : 0.480000e-02
Beam pattern filename : mns55.bpt
Beam power : 0.100000e+01
Beam pattern width : 0.180000e+03
Source pulse length : 0.000000e+00
Refl. map filename : mnschkres16b.map
Center X coord. : 0.100000e+04
Center Y coord. : 0.100000e+04
Refl. map X length : 0.308730e+02
Refl. map Y length : 0.308730e+02
Xpixels : 0.160000e+02
Ypixels : 0.160000e+02
Background refl. : 0.400000e-01
Camera X pos. : -0.414000e+00
Camera Y pos. : 0.000000e+00
Camera Z pos. : 0.486900e+01
Camera alpha : 0.000000e+00
Camera beta : -0.225000e+02
Camera gamma : 0.000000e+00
Source #1 X pos. : -0.161900e+01
Source #1 Y pos. : 0.319000e+00
Source #1 Z pos. : 0.472200e+01
Source #1 alpha : 0.000000e+00
Source #1 beta : -0.950007e+01
Source #1 gamma : 0.000000e+00
Source #2 X pos. : -0.161900e+01
Source #2 Y pos. : -0.319000e+00
Source #2 Z pos. : 0.472200e+01
Source #2 alpha : 0.000000e+00
Source #2 beta : -0.950007e+01
Source #2 gamma : 0.000000e+00
Rows output : 0.480000e+02
Columns output : 0.640000e+02
Backscatter planes : 0.100000e+02
Auto-aim (on,off) : off
Source conv. (fft,c) : fft
Glow conv. (fft,c) : fft
Vehicle filename : none
Vehicle X pos. : 0.000000e+00
Vehicle Y pos. : 0.000000e+00
Vehicle Z pos. : 0.000000e+00

Component factor : 0.111560e-04
Source factor : 0.506790e-02
  
```



<i>atten.'s</i> \H ₂ O	3.3m ⁻¹	6.6m ⁻¹	20m ⁻¹
1	$\frac{1920}{11880}$	$\frac{2160}{10980}$	$\frac{864}{5040}$
2	$\frac{1536}{10440}$	$\frac{1776}{6840}$	$\frac{576}{3420}$
3	$\frac{1248}{9540}$	$\frac{1536}{8100}$	$\frac{576}{3420}$

Table 3
 Conversion factors for converting UNCLES output to lux.
 Upper figure is for incandescent lights,
 lower figure is for thalium iodide.

α	UNCLES OUTPUT	altitude(m)	$N_w(ThalliumIodide)$	$E_c(lux)$
$3m^{-1}$	1.25×10^{-6}	9	.53	1.13×10^{-2}
$6.6m^{-1}$	7.66×10^{-7}	14	.63	8.15×10^{-3}
$20m^{-1}$	5.87×10^{-7}	30	.22	2.2×10^{-3}

Table 4:
Power Requirements for Optimal Configurations

α	.3	.3	.15	.49
$\frac{s}{\alpha}$.83	.83	.74	.61
file	UR9ABN	UR6N	US14AN	UT35ABCN
$\frac{\partial C_t}{\partial \alpha}$	-2.76		-2.53	-.801
$\frac{\partial C_t}{\partial \frac{s}{\alpha}}$	-.196	-.144		-.163

Table 5:

Results of UNCLES Sensitivity Study

Bibliography

Ballard,D.H. and D.M. Brown, Computer Vision, Prentice-Hall Inc., Englewood Cliffs, New Jersey,(1982).

Duntley, S.Q.,Light in the Sea,J. Opt. Soc. Am. 53 (1963).

Chilton,F.,D.D. Jones and W.K. Talley,Imaging Properties by the Sea,J. Opt. Soc. Am.,59,8,(1969).

Dixon,T.H.,T.J. Piviritto,R.F. Chapman and R.C. Tyce, A Range- Gated Laser System for Ocean Floor Imaging, MTS Journal, 17,4,(1983)

Funk,C.J., Bryant,S.B. and P.J. Heckman Jr.,Handbook of Underwater Imaging System Design, Ocean Technology Dept. NUSC (1973)

Gordon,A. and M.R. Knittel,Underwater Multiple Scattering of Light for System Designers,NUC TP371,(1973).

Jaffe, J.S.,The Domains of Underwater Visibility,SPIE Ocean Optics VIII, April 1986.

McGlamery,B.J.,A Computer Model for Underwater Camera Systems, SPIE,V28,Ocean Optics VI, S.Q. Duntley, ed.,(1979).

Preisendorfer,R.W,Hydrological Optics,Vol II,Foundations, U.S. Dept. of Commerce,1976.

RCA Electro-Optics Handbook, RCA,Solid State Division, Electro Optics and Devices.Lancaster PA 17604(1974).

Rosenfeld and A..A. Kak Digital Picture Processing. (Academic Press,Inc.,New York)(1982).

Wells, W.H.,Loss of Resolution in Water as a Result of Multiple Small-Angle Scattering, J. Opt. Soc. Am.,59,(1969).

Xybion Model ISG-01 Gated Intensified Solid-State (CID) Video Camera (1987). Xybion Electronic Systems Corporation,7750-A Convoy Court,San Diego CA. 92111

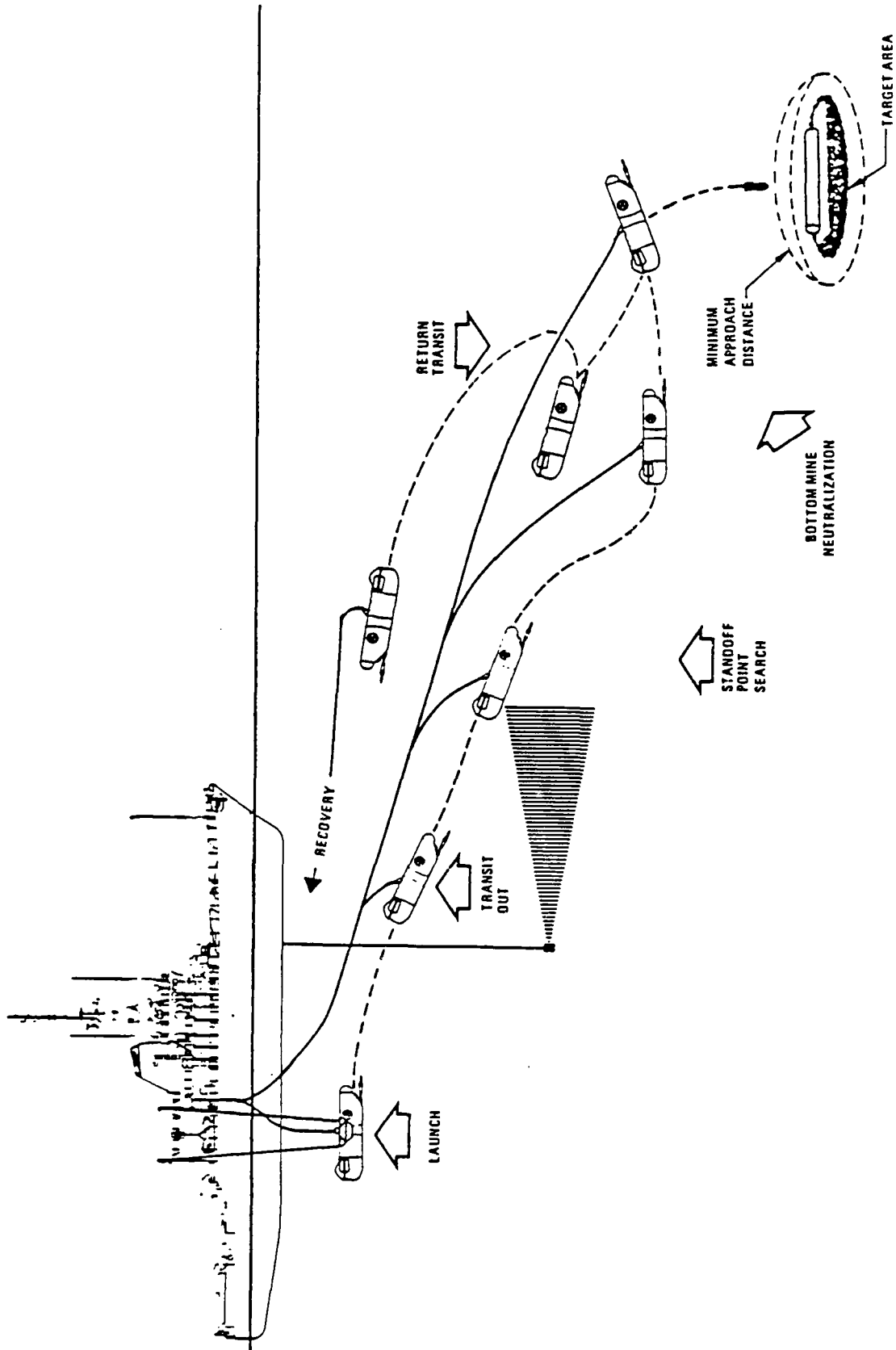


Figure 1: Bottom Mine Neutralization

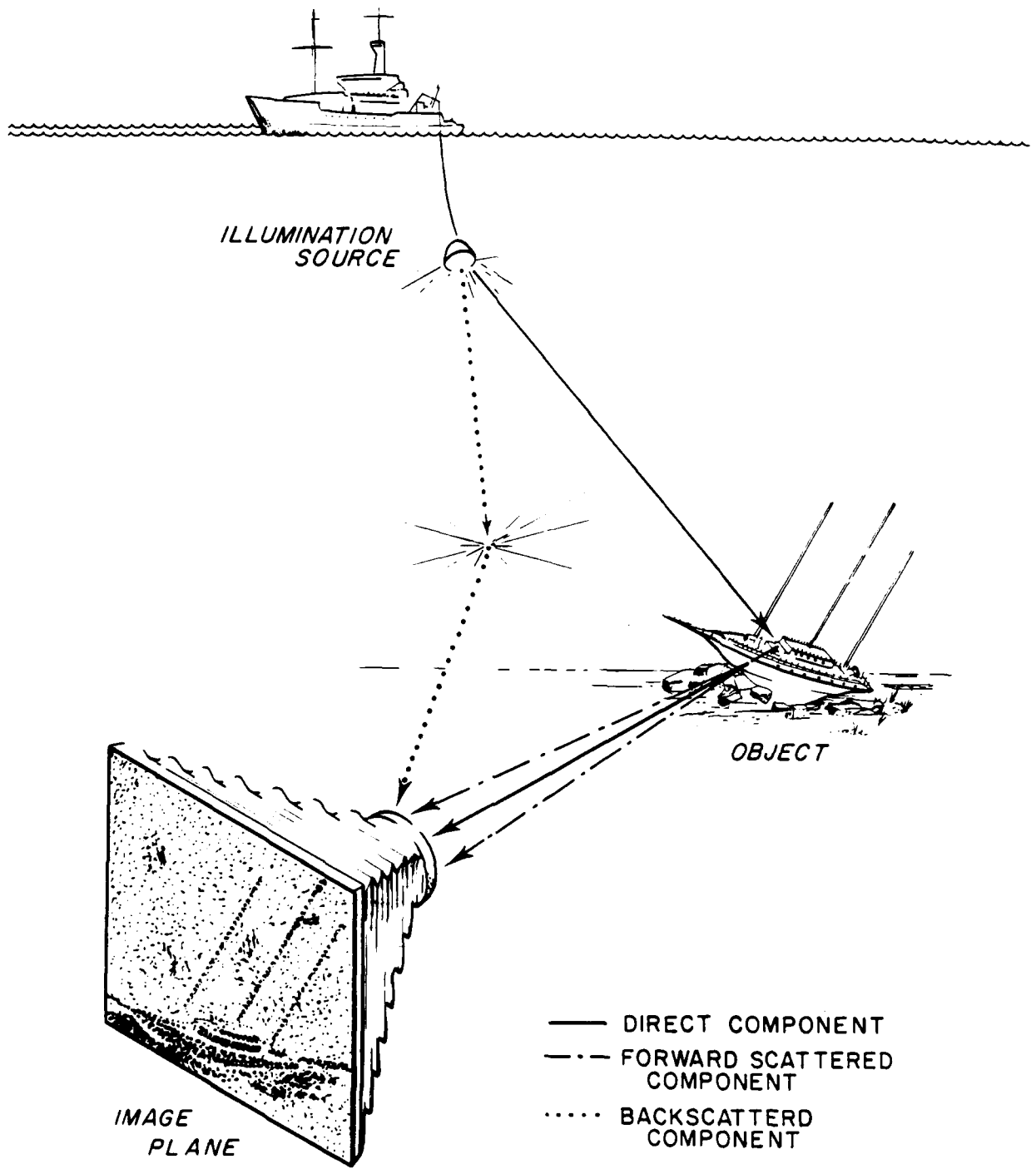
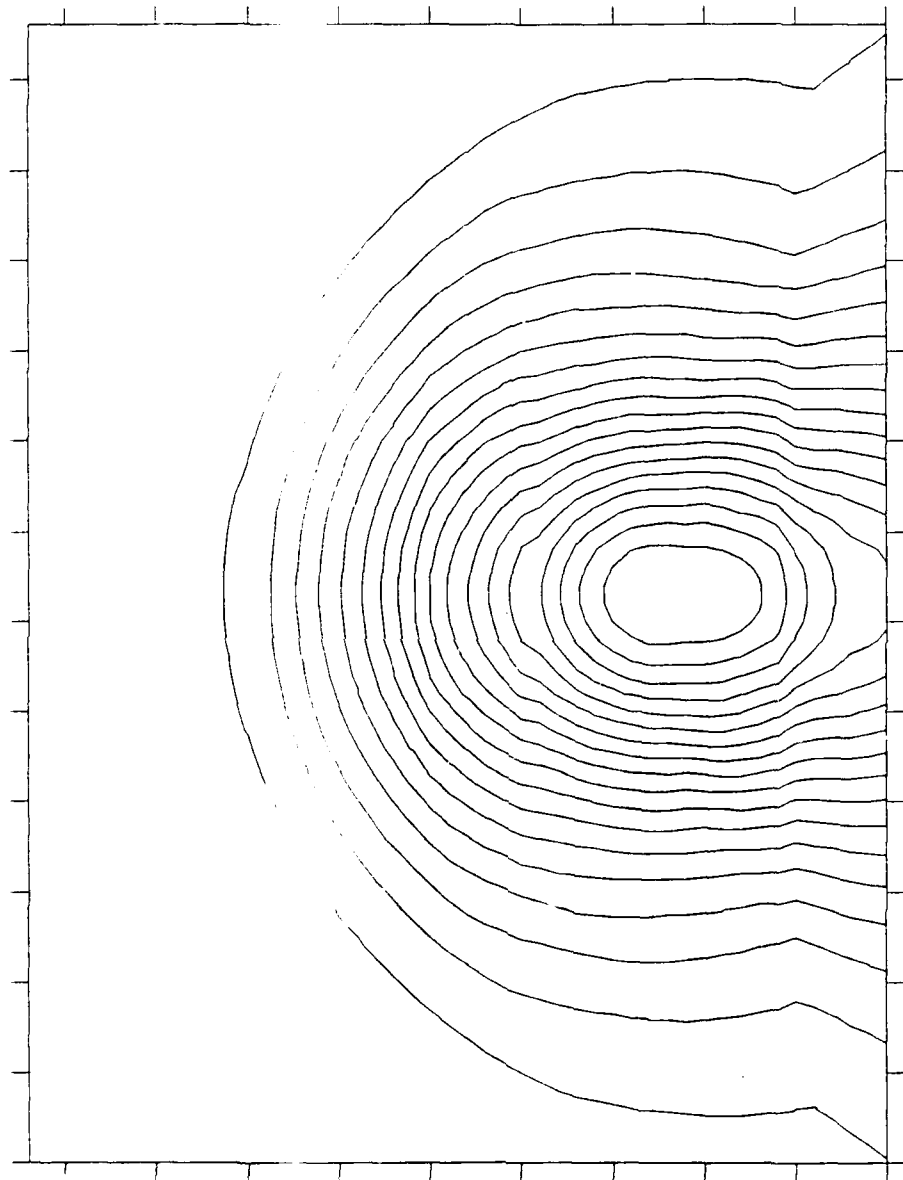


Figure 2: The Components of An Imaging Experiment



3/29/1988 14:17:39 ur4.5q factor= 0.111560e-04
contour levels: 0.334e-08 to 0.112e-04 by 0.587e-0

Figure 3: total comp.

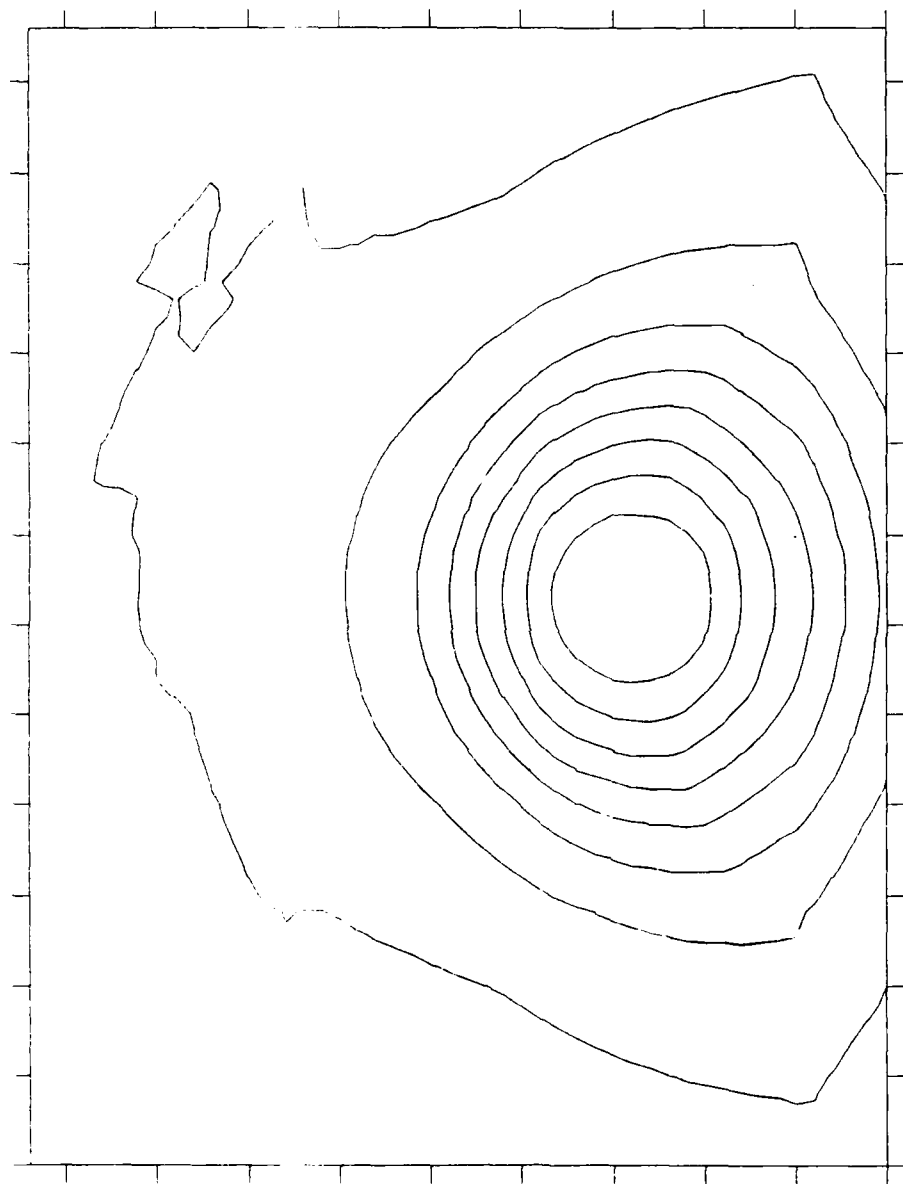
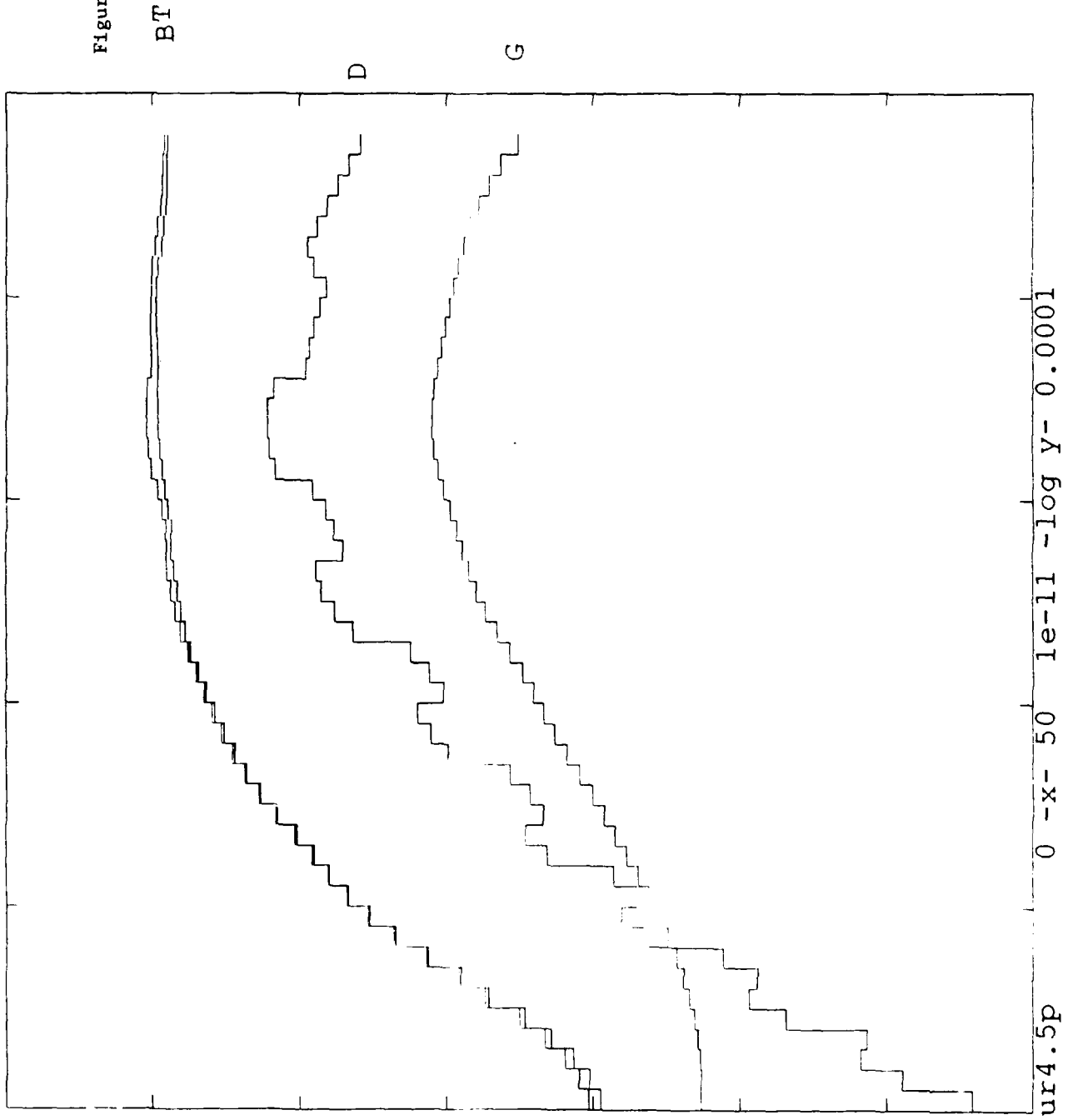


Figure 4: contrast xmittance
3/29/1988 14: 9:10 ur4.5q
contour levels: 0.378e-03 to 0.157e+00 by 0.174e-0

Figure 5: A Slice Plot



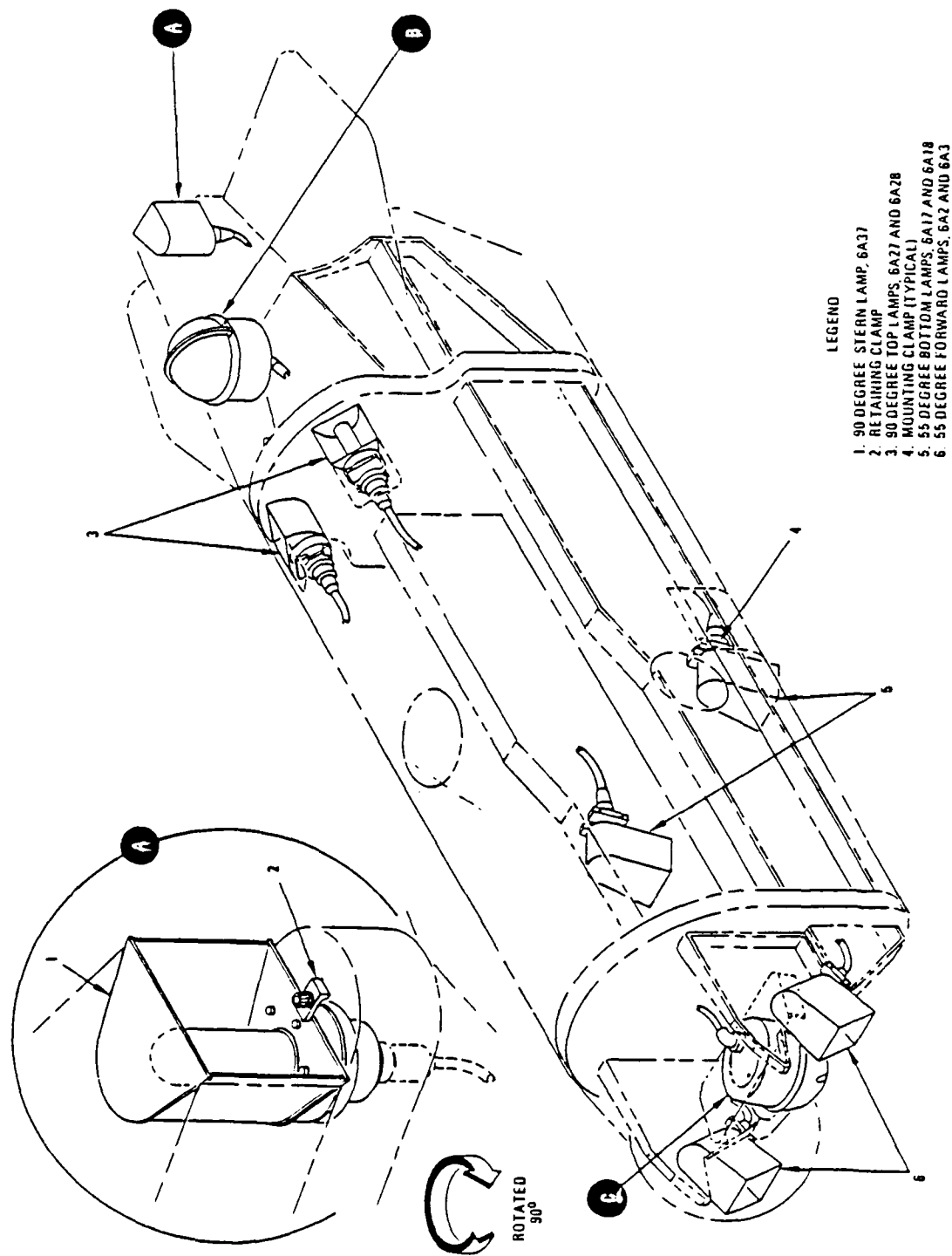


Figure 6: TV Camera and Light Installation

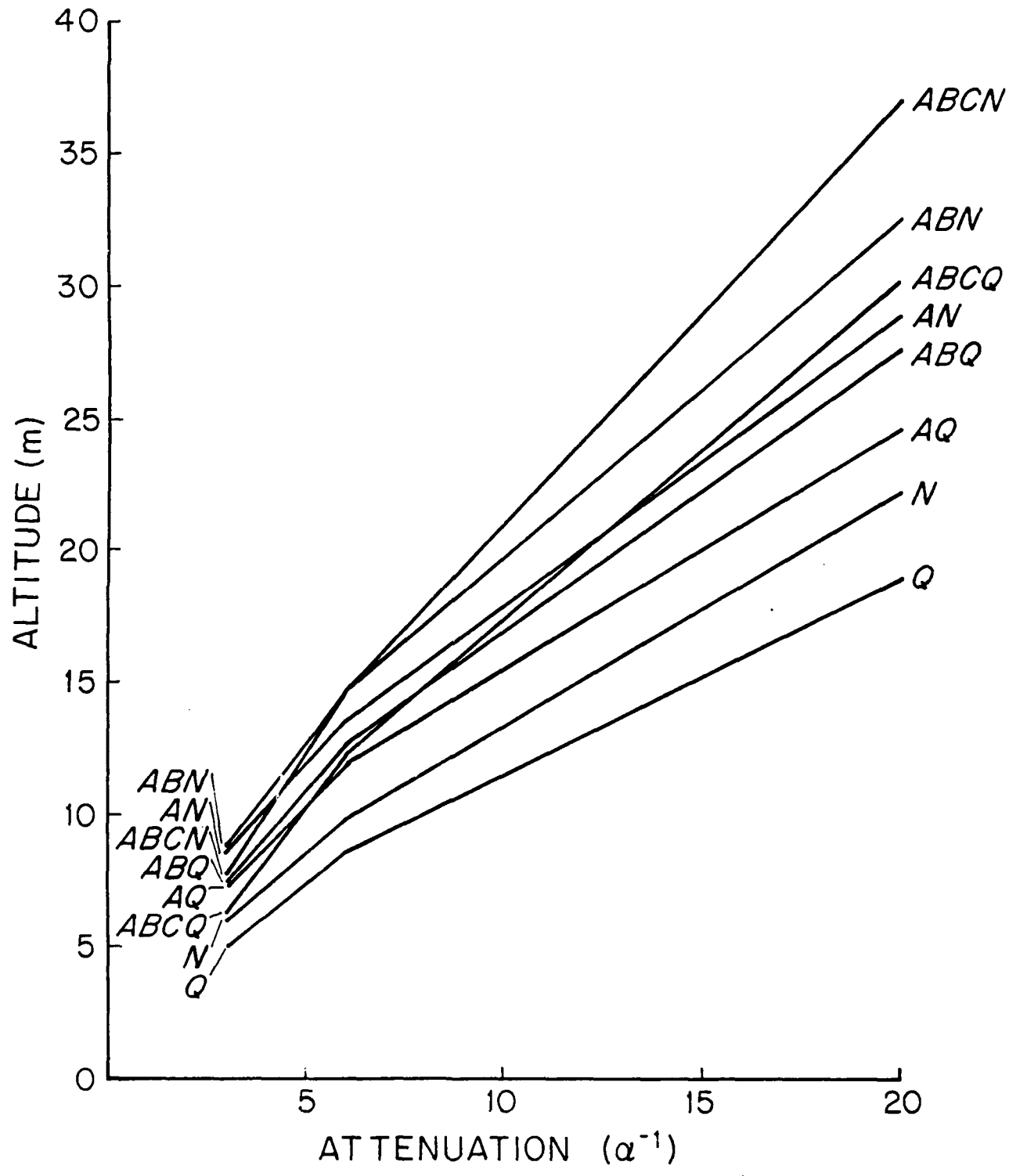


Figure 7: Summary of Project Results

PERCENTAGE AREA COVERED AT ≥ 0.02 CT

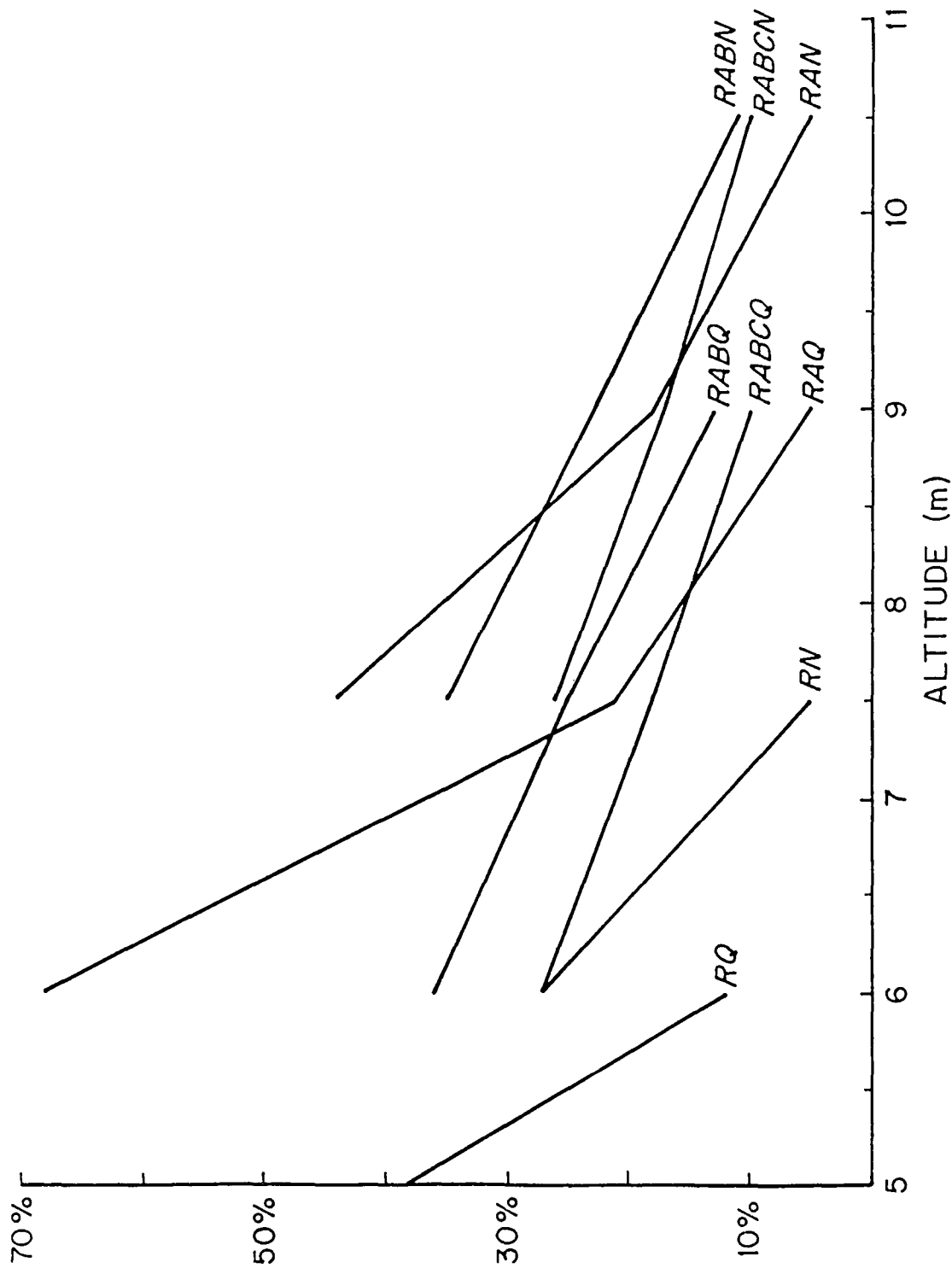


Figure 7a: Interpolation Curves for 3 Meter Water

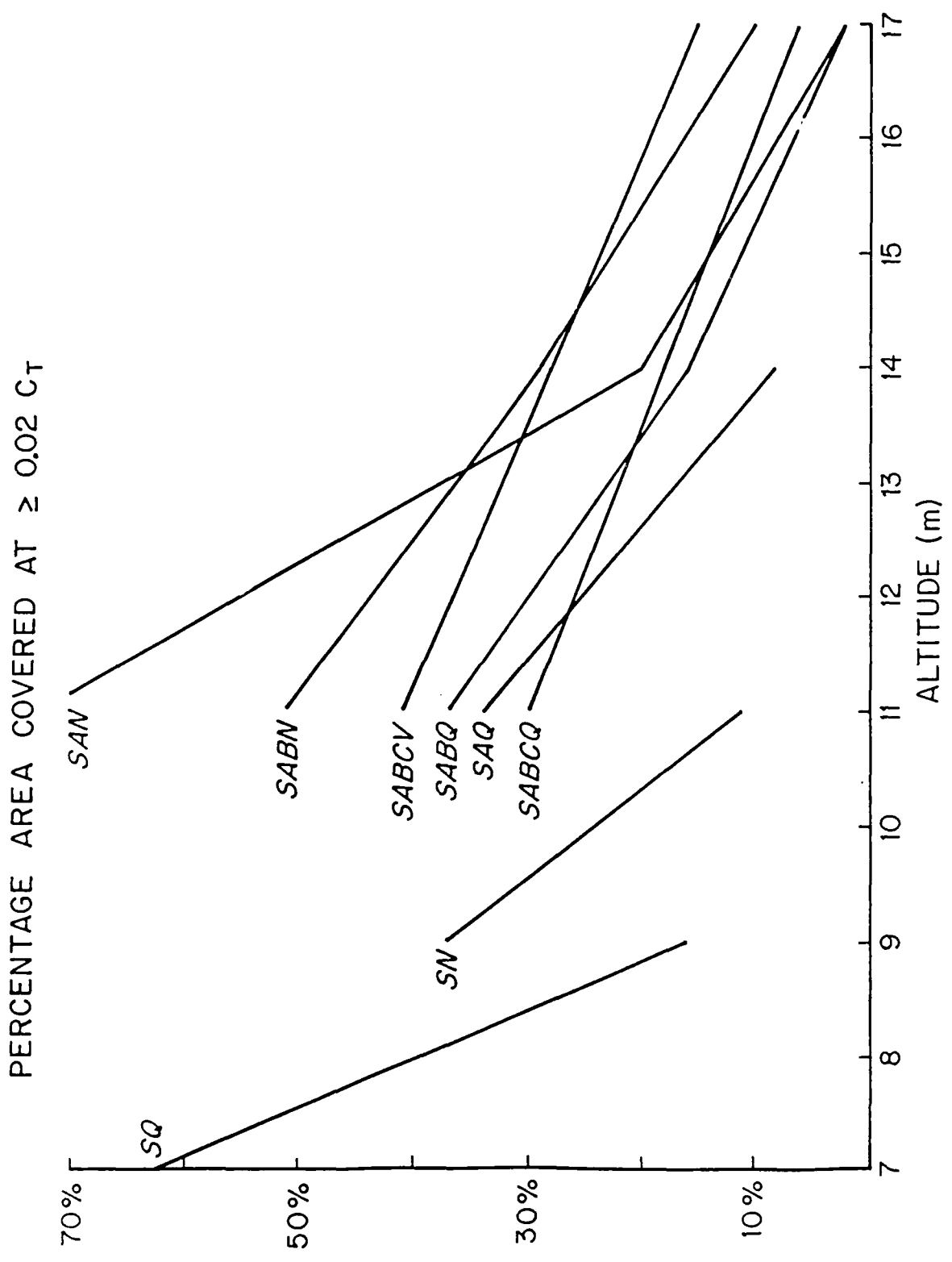


Figure 7b: Interpolation Curves for Six Meter Water

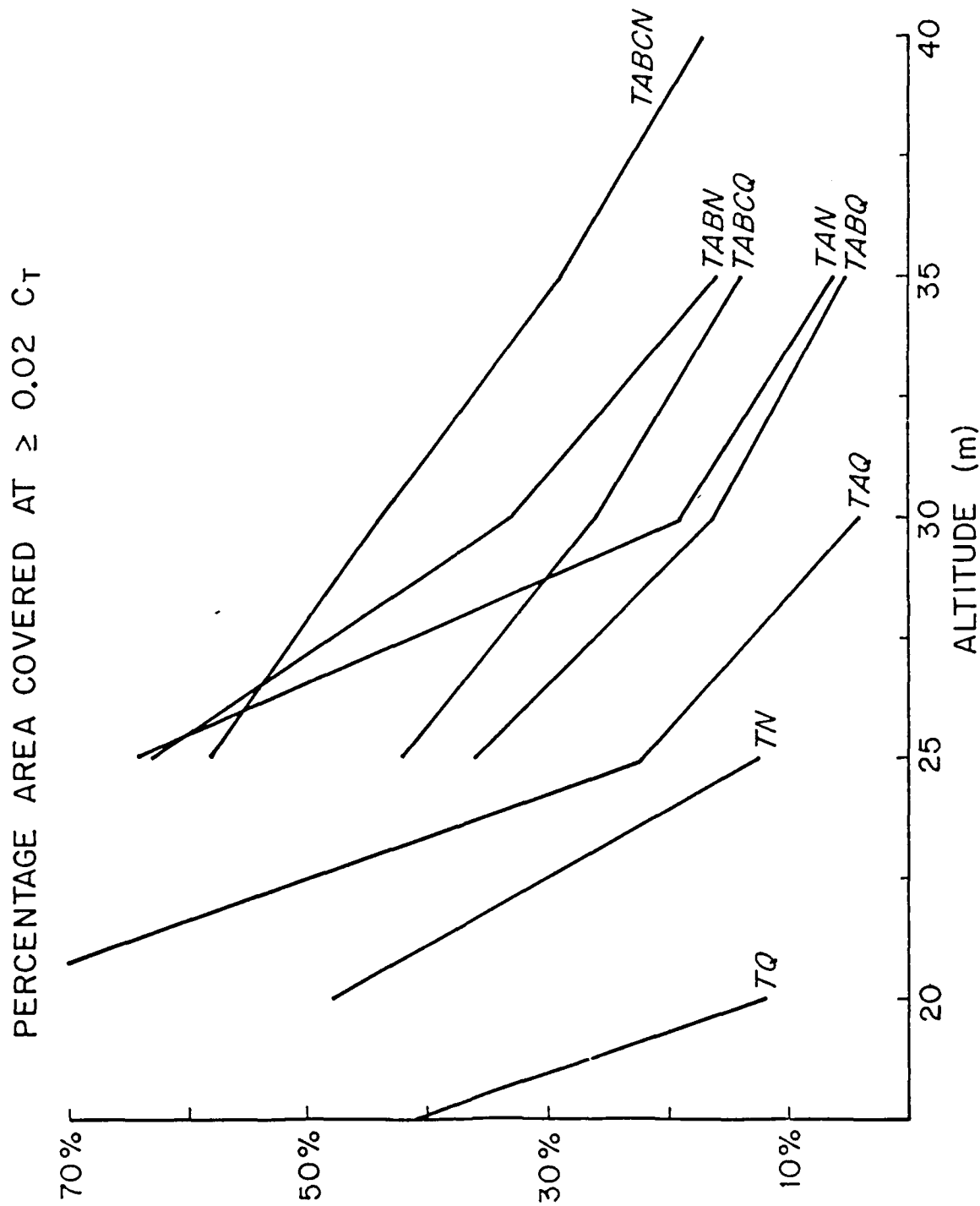


Figure 7c: Interpolation Curves for Twenty Meter Water

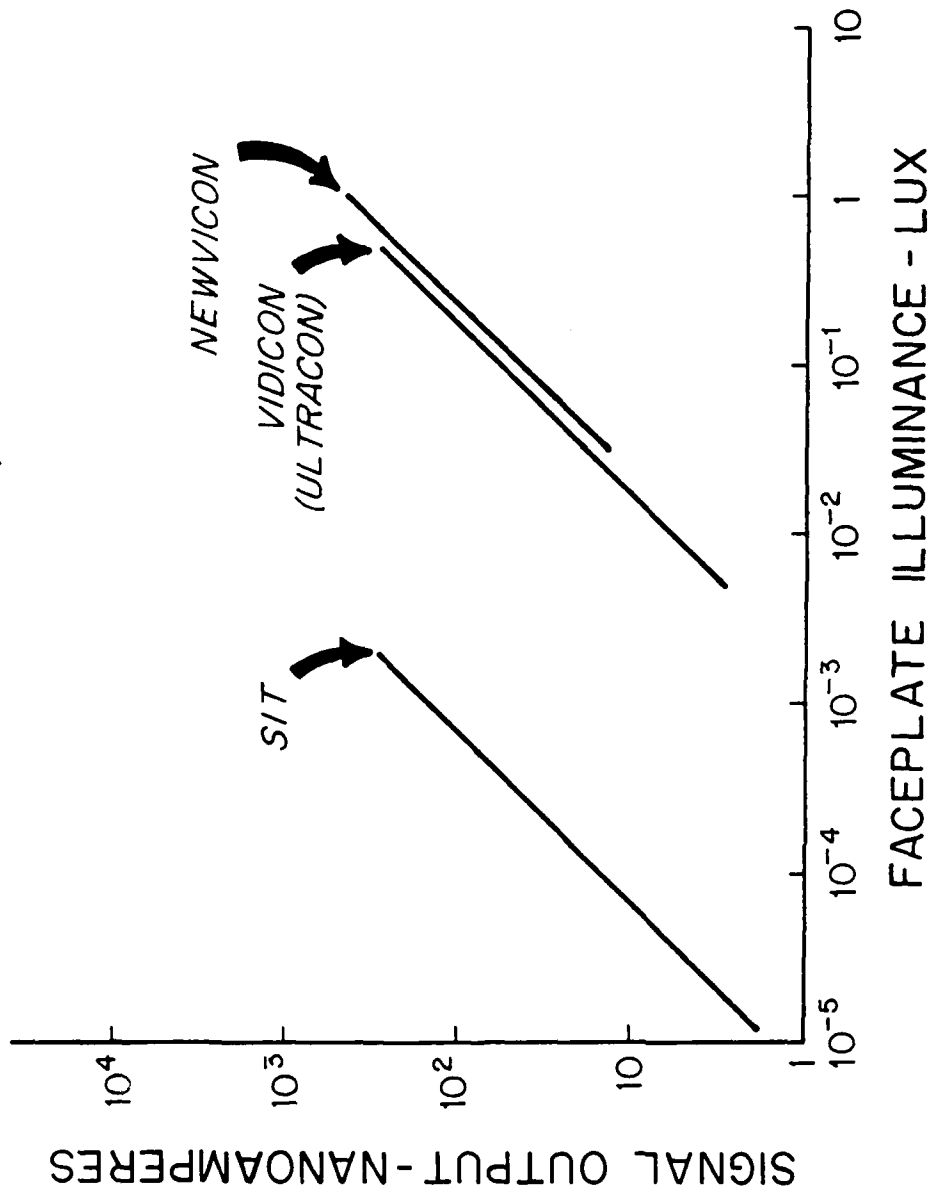


Figure 8: Camera Sensitivity Curves

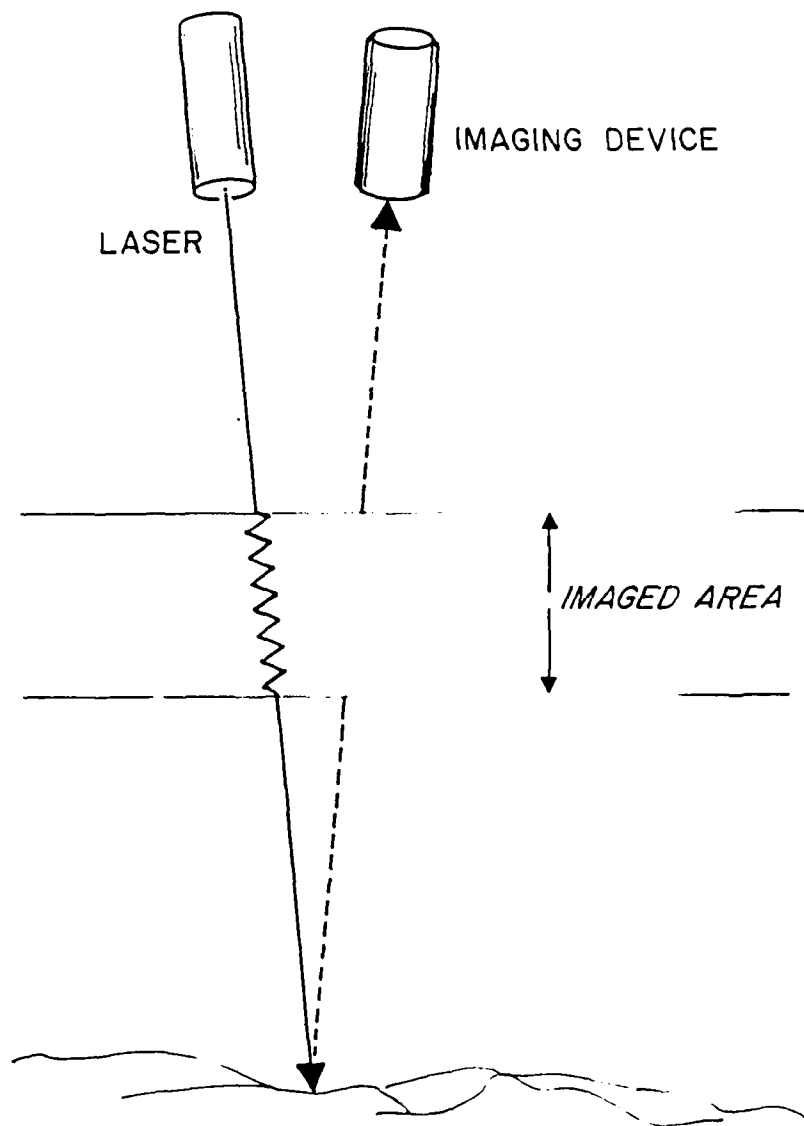


Figure 9: RANGE GATED IMAGERY

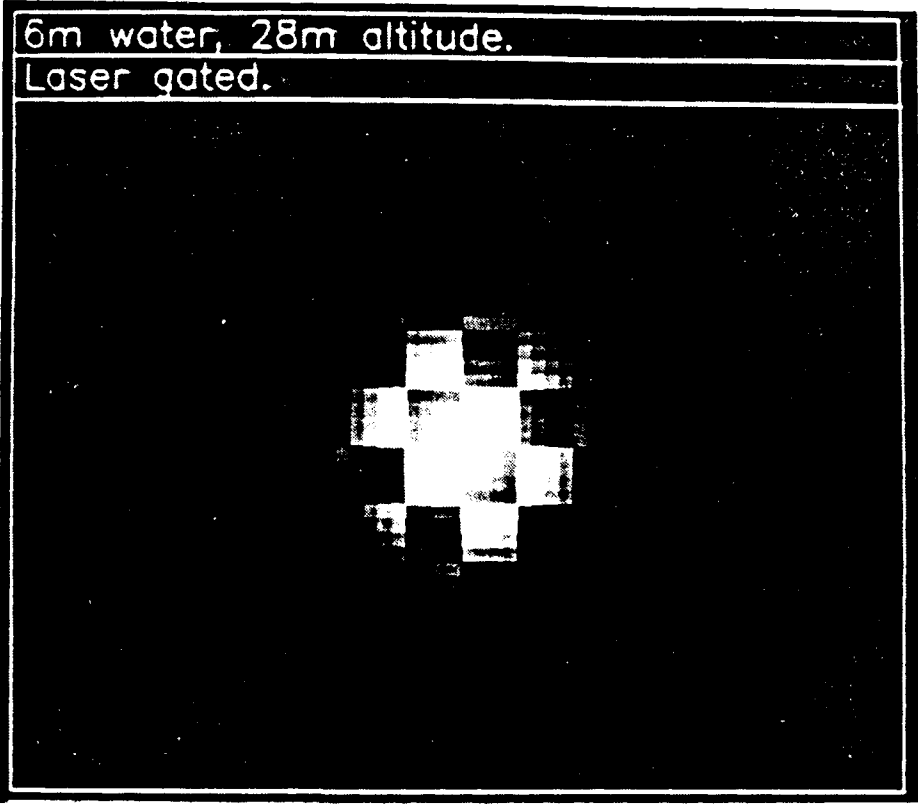


Figure 10:A Range-Gated Image

RANGE GATED SYSTEMS PERFORMANCE

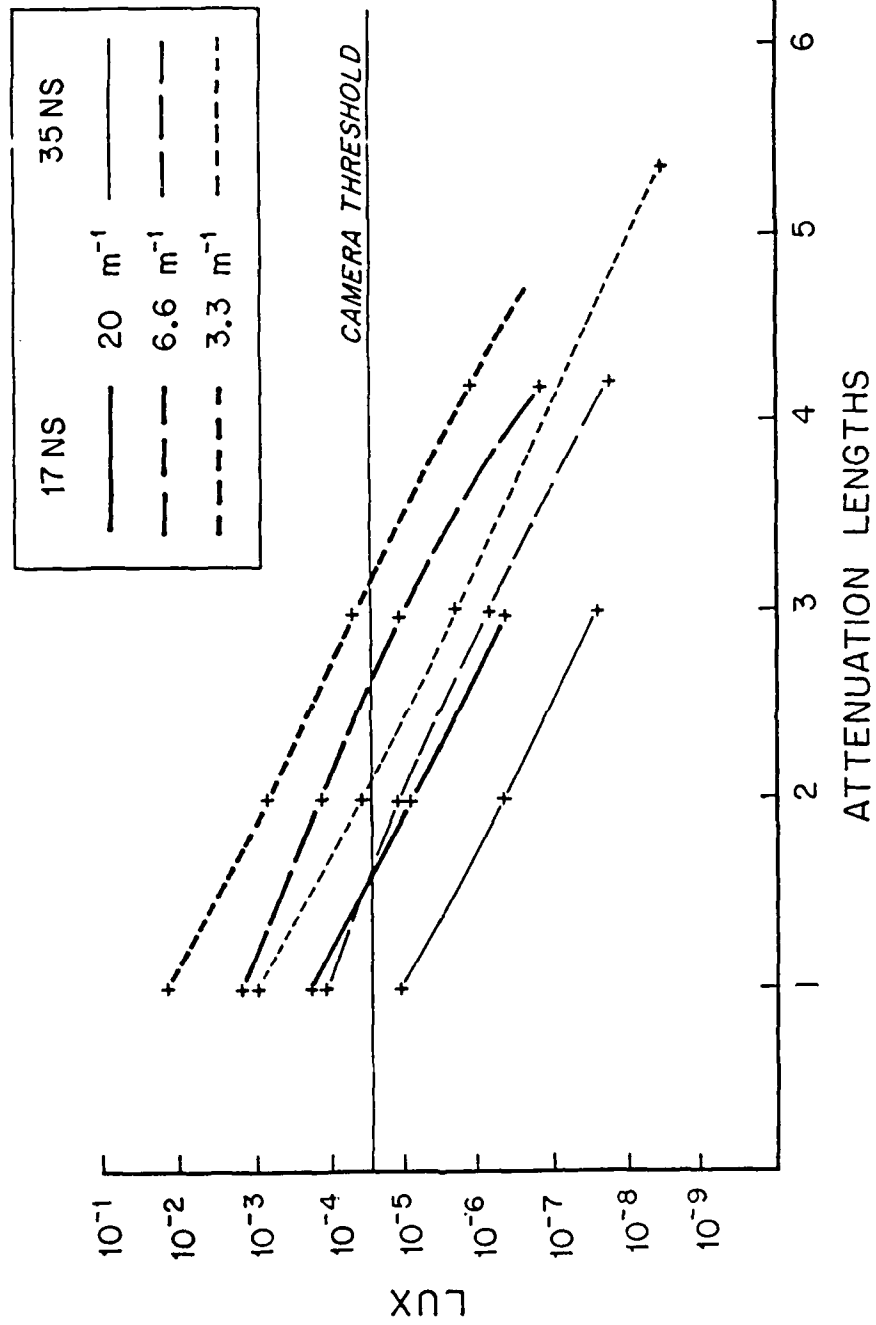


Figure 11: Range-Gated Power Curves

RECEIVING GEOMETRY

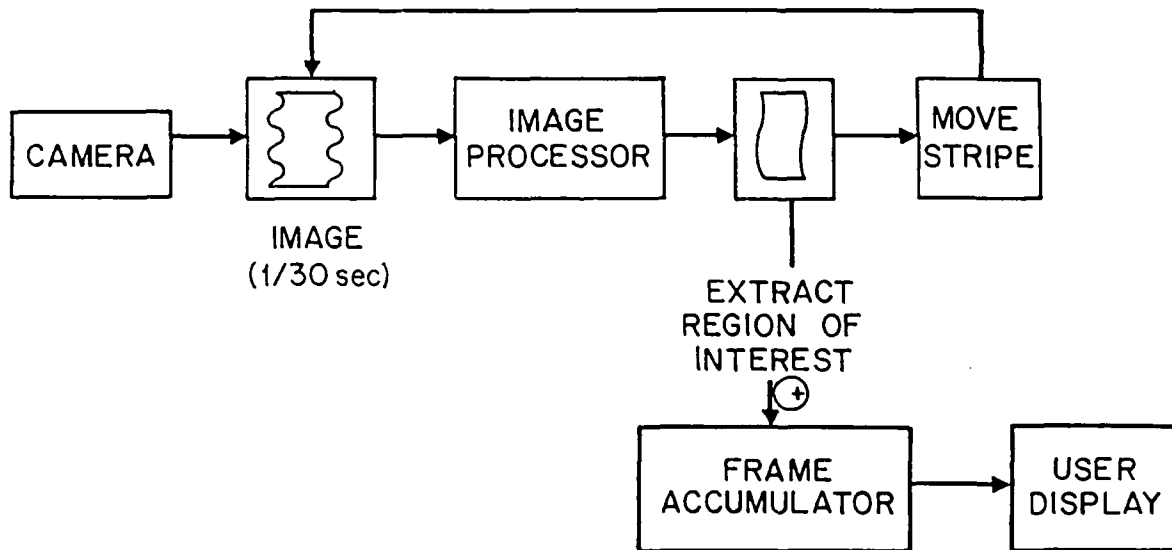
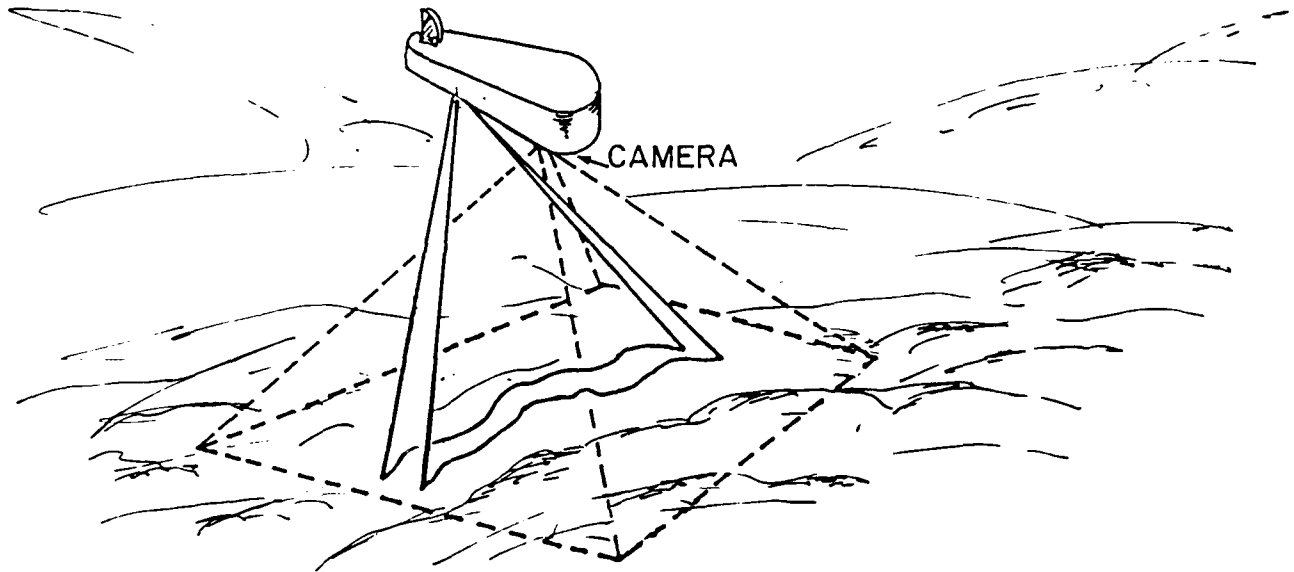


IMAGE PROCESSING

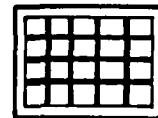


Figure 12: IMAGE FORMATION VIA STRIPED ILLUMINATION

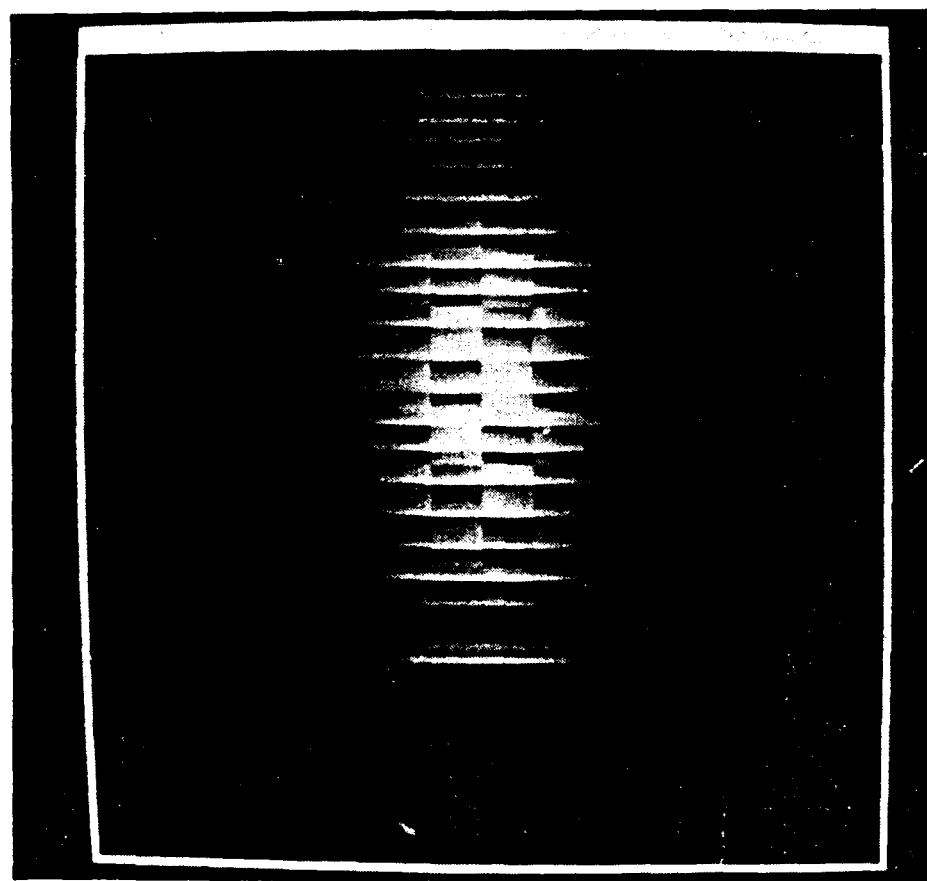


Figure 13:A Light Striped Image

AMBIENT LIGHTING STUDY

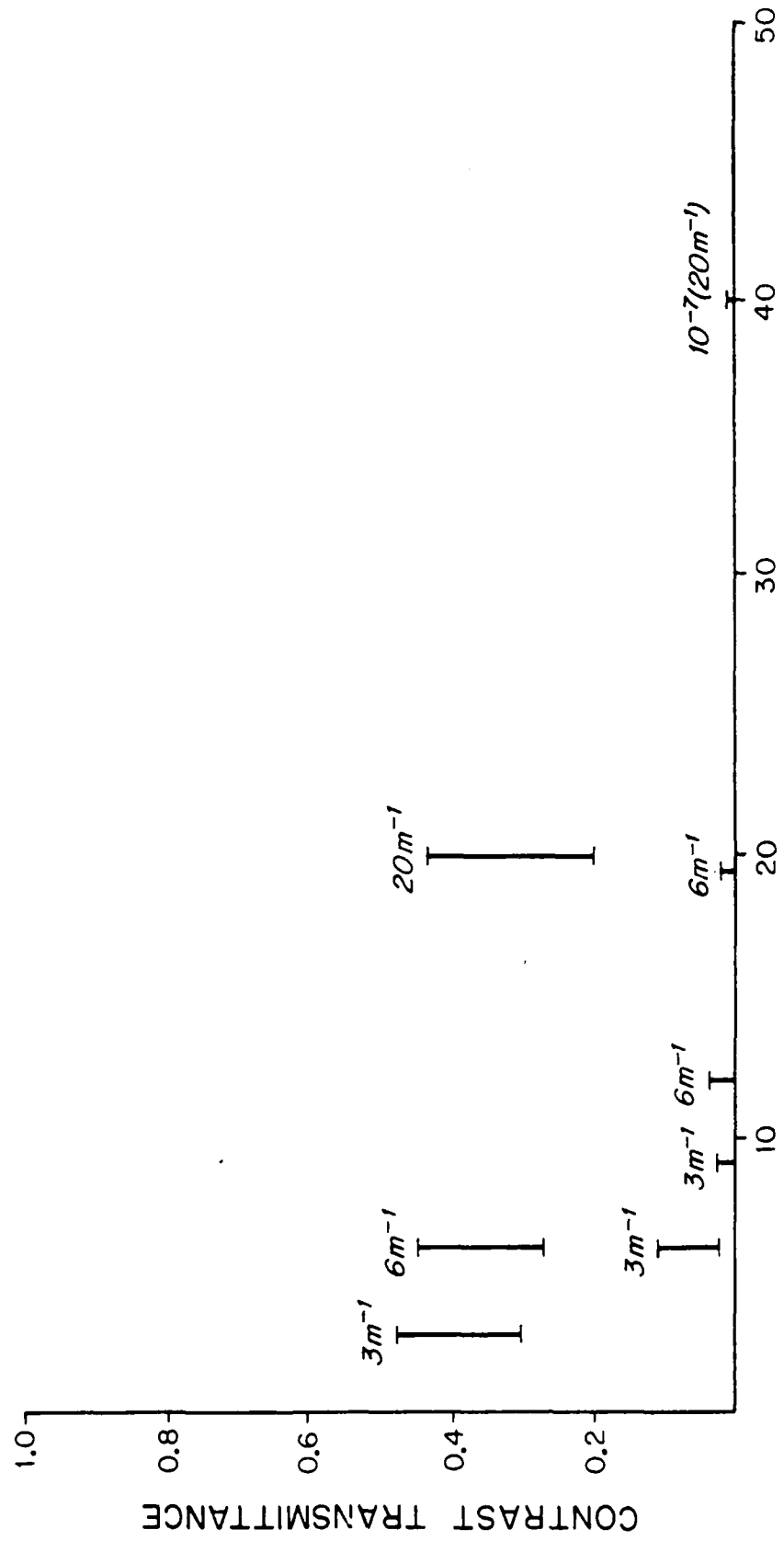
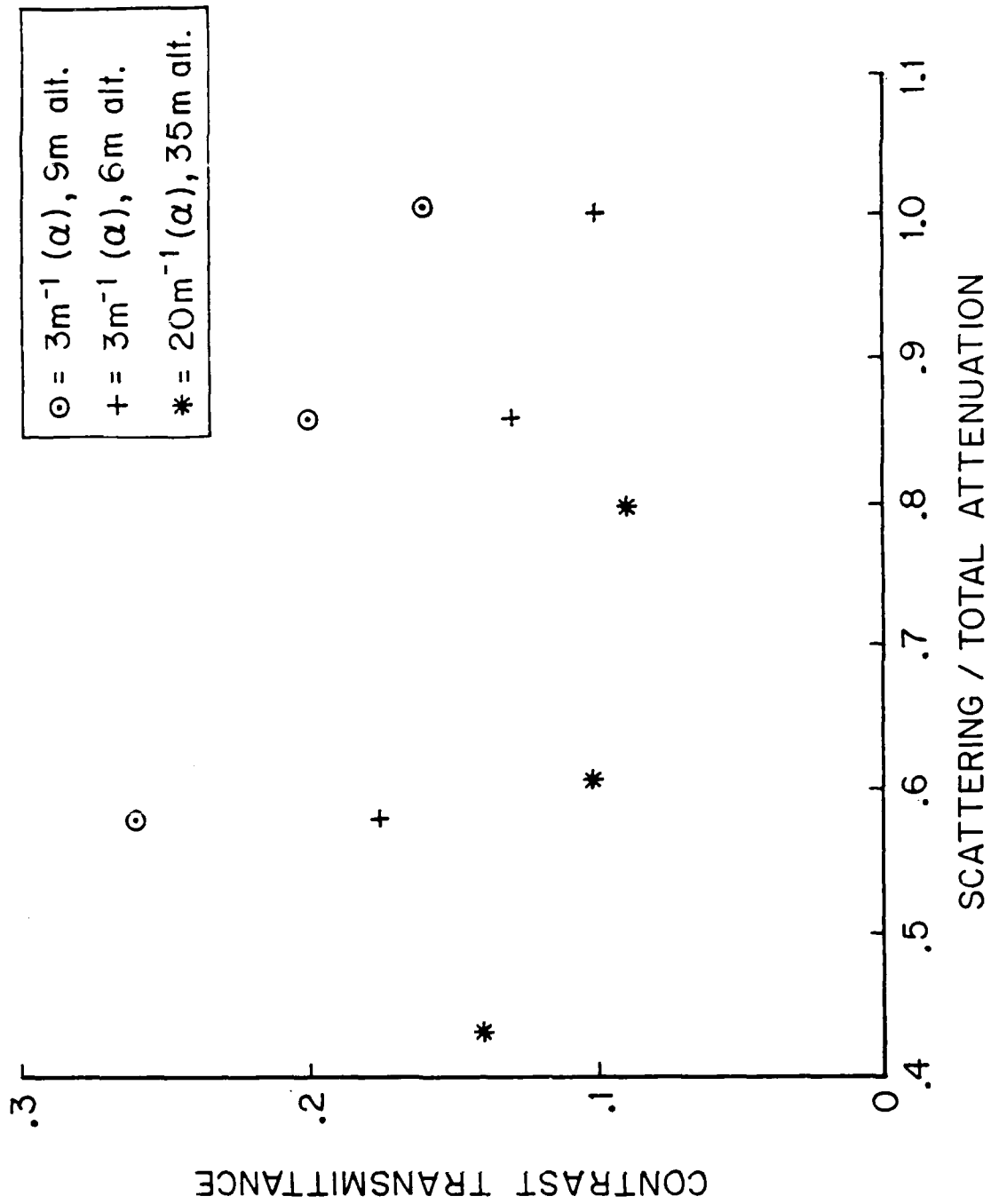


Figure 14: Results of the Ambient Lighting Study

Figure 15: RESULTS of SENSITIVITY STUDY:

Contrast Transmittance (C_T) vs Scattering / Total Attenuation (S/α)



DOCUMENT LIBRARY

August 9, 1988

Distribution List for Technical Report Exchange

Attn: Stella Sanchez-Wade
Documents Section
Scripps Institution of Oceanography
Library, Mail Code C-075C
La Jolla, CA 92093

Hancock Library of Biology &
Oceanography
Alan Hancock Laboratory
University of Southern California
University Park
Los Angeles, CA 90089-0371

Gifts & Exchanges
Library
Bedford Institute of Oceanography
P.O. Box 1006
Dartmouth, NS, B2Y 4A2, CANADA

Office of the International
Ice Patrol
c/o Coast Guard R & D Center
Avery Point
Groton, CT 06340

Library
Physical Oceanographic Laboratory
Nova University
8000 N. Ocean Drive
Dania, FL 33304

NOAA/EDIS Miami Library Center
4301 Rickenbacker Causeway
Miami, FL 33149

Library
Skidaway Institute of Oceanography
P.O. Box 13687
Savannah, GA 31416

Institute of Geophysics
University of Hawaii
Library Room 252
2525 Correa Road
Honolulu, HI 96822

Library
Chesapeake Bay Institute
4800 Atwell Road
Shady Side, MD 20876

MIT Libraries
Serial Journal Room 14E-210
Cambridge, MA 02139

Director, Ralph M. Parsons Laboratory
Room 48-311
MIT
Cambridge, MA 02139

Marine Resources Information Center
Building E38-320
MIT
Cambridge, MA 02139

Library
Lamont-Doherty Geological
Observatory
Columbia University
Palisades, NY 10964

Library
Serials Department
Oregon State University
Corvallis, OR 97331

Pell Marine Science Library
University of Rhode Island
Narragansett Bay Campus
Narragansett, RI 02882

Working Collection
Texas A&M University
Dept. of Oceanography
College Station, TX 77843

Library
Virginia Institute of Marine Science
Gloucester Point, VA 23062

Fisheries-Oceanography Library
151 Oceanography Teaching Bldg.
University of Washington
Seattle, WA 98195

Library
R.S.M.A.S.
University of Miami
4600 Rickenbacker Causeway
Miami, FL 33149

Maury Oceanographic Library
Naval Oceanographic Office
Bay St. Louis
NSTL, MS 39522-5001

Marine Sciences Collection
Mayaguez Campus Library
University of Puerto Rico
Mayaguez, Puerto Rico 00708

REPORT DOCUMENTATION PAGE	1. REPORT NO. WHOI-88-33	2.	3. Recipient's Accession No.
4. Title and Subtitle Underwater Imaging System Performance Characterization		5. Report Date August 1988	
7. Author(s) Jules S. Jaffe		6.	
9. Performing Organization Name and Address The Woods Hole Oceanographic Institution Woods Hole, Massachusetts 02543		8. Performing Organization Rept. No. WHOI-88-33	
12. Sponsoring Organization Name and Address The Office of Naval Research Environmental Sciences Directorate Arlington, VA 22217		10. Project/Task/Work Unit No.	
15. Supplementary Notes This report should be cited as: Woods Hole Oceanog. Inst. Tech. Rept., WHOI-88-33.		11. Contract(C) or Grant(G) No. (C) N00011-86-C-0344 (G)	
16. Abstract (Limit: 200 words) This report summarizes the results of a computer study that was initiated in order to study the performance and recommend possible improvements to the Mine Neutralization Vehicle System. The computer model UNCLES which was written by the Woods Hole Oceanographic Institution was used for this purpose. The results indicate that as currently configured, the vehicle will be able to see no more than 1 attenuation length in range. The study of the possible improvements in vehicle configuration indicate that large improvements in image visibility can be had for small changes in camera/light configurations. Movement of the lights aft, narrowing of the beam patterns, and adjustment of the pointing angles can be used to double the imaging performance in almost all environmental conditions. Additional studies of advanced sensors indicate that the current generation of commercial lasers are too low in power to permit extended visibility. As a means of extending the imaging range of the vehicle a system that employs scanning light beams in concert with image processing is suggested. The computer simulations of this configuration indicate that visibility to 5 attenuation lengths will be possible with this system.		13. Type of Report & Period Covered Technical Report	
17. Document Analysis a. Descriptors 1. Underwater imaging 2. Computer simulation 3. Remote vehicles b. Identifiers/Open-Ended Terms c. COSATI Field/Group		14.	
18. Availability Statement Approved for publication; distribution unlimited.		19. Security Class (This Report) UNCLASSIFIED	21. No. of Pages 48
		20. Security Class (This Page)	22. Price